Beneficial reversal of dominance maintains a resistance polymorphism under fluctuating insecticide selection

Marianthi Karageorgi[1,7], Anastasia S. Lyulina[1,2], Mark C. Bitter[1], Egor Lappo[1], Sharon I. Greenblum[3], Zach K. Mouza[1], Caitlynn T. Tran[1], Andy V. Huynh[1], Hayes Oken[4], Paul Schmidt[4,6,7], and Dmitri A. Petrov[1,5,6,7]

1. Department of Biology, Stanford University, Stanford, CA 94305, USA
2. Department of Applied Physics, Stanford University, Stanford, CA 94305, USA
3. Department of Energy Joint Genome Institute, Lawrence Berkeley National Laboratory, Berkeley, CA 94720, USA
4. Department of Biology, University of Pennsylvania, Philadelphia, PA 19104, USA
5. CZ Biohub, San Francisco, CA 94158
6. These authors contributed equally
7. Corresponding authors: M.K. (mkarag@stanford.edu), P.S. (schmidtp@upenn.edu), and D.A.P (dpetrov@stanford.edu)

Abstract

Large-effect functional genetic variation is commonly found in natural populations, even though natural selection should erode such variants. Theory suggests that under fluctuating selective pressures, beneficial reversal of dominance - where alleles are dominant when beneficial and recessive when deleterious - can protect these loci from selection, allowing them to persist. However, empirical evidence for this mechanism remains elusive because testing requires direct measurements of selection and dominance in natural conditions. Here, we show that insecticide-resistant alleles at the *Ace* locus in *Drosophila melanogaster* persist worldwide at intermediate frequencies and exhibit beneficial reversal of dominance. By combining laboratory and large-scale field mesocosm experiments with insecticide manipulation, and mathematical modeling, we show that the benefits of the resistant *Ace* alleles are dominant while their fitness costs recessive. We further show that fluctuating insecticide selection generates chromosome-scale genomic perturbations at sites linked to the resistant *Ace* alleles, revealing broader genomic consequences of this mechanism. Overall, our results suggest that beneficial reversal of dominance contributes to the maintenance of functional genetic variation and impacts patterns of genomic diversity via linked fluctuating selection.

Main text

Large-effect functional variants responding to temporally fluctuating selective pressures persist in natural populations across taxa, from ancient to recently evolved polymorphisms to anthropogenic pressures[1,2]. A striking example comes from studies of seasonal dynamics in *Drosophila*, where alleles can change frequencies by tens of percent per season[3–6] yet remain polymorphic over millions of generations[3]. However, their maintenance is puzzling because population genetics theory suggests that the conditions for preserving functional genetic variation under temporally fluctuating selection are restrictive[7]. One mechanism that can relax these conditions is beneficial reversal of dominance[8,9], where alleles are partially or completely dominant when beneficial in favorable environments but become partially or completely recessive when deleterious in unfavorable environments[10,11]. This mechanism acts as a stabilizing force, protecting recessive deleterious alleles from selection while enabling rapid adaptation when selection shifts. An extension of Wright's physiological theory of dominance[12] further suggests that this reversal can occur when alternative adaptive alleles at a locus function as loss-of-function variants in their unfavored environments[10]. However, empirical evidence for the mechanism remains scarce because testing requires direct measurements of selection and dominance of adaptive alleles on fitness in natural conditions.

The *Ace* locus in insects provides an ideal genetic system to test whether beneficial reversal of dominance can maintain functional variation under fluctuating selection[13]. *Ace* encodes acetylcholinesterase (AChE), a key enzyme in the insect nervous system responsible for breaking down acetylcholine[13,14]. Organophosphate insecticides, introduced in the 1950s and 1960s, act as irreversible inhibitors of AChE, causing insect death by binding to its active site

57 and preventing removal of acetylcholine from the synapses upon firing[15]. These insecticides have
58 imposed seasonally fluctuating selection pressures on resistant insect populations, as seen in
59 seasonal resistance fluctuations in field studies[16–18]. Following Wright's physiological theory of
60 dominance, resistant alleles should be loss-of-function and thus recessive in pesticide-free
61 environments, while sensitive alleles should become loss-of-function and thus recessive in
62 pesticide-rich environments[19,20]. Consistent with this prediction, previous studies across resistant
63 insect populations suggest that resistant *Ace* alleles follow patterns of beneficial reversal of
64 dominance often showing dominant benefits and/or recessive costs for fitness-associated
65 traits[19,21], though direct evidence is lacking.

66 Here, we test whether beneficial reversal of dominance under temporally fluctuating
67 selection contributes to the maintenance of the resistant *Ace* alleles in natural populations of *D.*
68 *melanogaster*, and investigate the broader genomic consequences of the mechanism. In
69 *Drosophila melanogaster*, resistant *Ace* alleles have repeatedly evolved in natural populations in
70 response to organophosphate selection[22,23], and enzymatic assays suggest the resistance
71 mutations are beneficial under insecticide exposure and costly in its absence[22,24]. However, the
72 phenotypic and fitness consequences of these mutations have not been studied. We combine
73 population genomic analysis, laboratory assays, and a novel field mesocosm system that enables
74 real-time tracking of genome-wide allele frequencies and resistance under controlled insecticide
75 manipulation[5] to test for beneficial reversal of dominance of the resistant *Ace* alleles. The field
76 mesocosm system establishes a direct experimental approach to observe beneficial reversal of
77 dominance and its genomic consequences in response to controlled selective pressures in semi-
78 natural conditions.

79 **Resistant *Ace* alleles persist in natural populations and respond to fluctuating insecticide**
80 **selection**

81 We first examined whether resistant *Ace* alleles exhibit signatures consistent with beneficial
82 reversal of dominance under temporally fluctuating selection in natural *D. melanogaster*
83 populations. This mechanism predicts that resistant *Ace* alleles should fluctuate in response to
84 temporally fluctuating selection while persisting at intermediate frequencies. Previous studies
85 identified resistant *Ace* alleles in *D. melanogaster* with mutations at four conserved sites near the
86 AChE active site (I161V, G265A, F330Y, G368A), with VGFG and VAYG as the most common
87 resistance haplotypes[22,23] (inset, **Fig. 1a**). Our analysis of inbred lines from Pennsylvania
88 (LNPA[5]) and North Carolina (DGRP[25]) confirmed these as the most common resistant
89 haplotypes in resistant *Ace* alleles (**Extended Data Fig. 1a, b**), with the LNPA also carrying
90 VGFA at ~13% frequency. Because I161V is present across the most common haplotypes, we
91 used it as a shared marker to track resistant *Ace* alleles in natural populations.

92 While resistant *Ace* alleles experience temporally fluctuating selection, they are also
93 subject to spatial variation in insecticide exposure. To disentangle these effects, we analyzed
94 genomic data from worldwide *D. melanogaster* populations from the Drosophila Evolution Over
95 Space and Time (DEST) database[26] and country-level pesticide use data from the Food and
96 Agricultural Organization of the United Nations (FAO)[27] (see **Methods f**or details). Spatially,
97 I161V frequency increases with pesticide use intensity across countries (linear mixed-effect
98 model, $p = 0.006$) (**Fig. 1a, b**) and shows stronger spatial variation compared to control SNPs
99 matched for recombination and average frequency ($p = 0.005$) (**Fig. 1c**). Temporally, seasonal
100 sampling at Linvilla Orchards, a non-organic farm where samples were collected in spring and

101 fall from 2009 to 2015, revealed a consistent fall-to-spring decline in I161V frequency
102 (generalized linear model, $p = 0.005$), suggesting either fitness costs of the resistant *Ace* alleles in
103 winter (insecticide-free time period) or seasonal migration (**Fig. 1d**). In addition, the I161V
104 polymorphism showed stronger temporal fluctuations than matched control SNPs ($p = 0.053$)
105 (**Fig. 1e).** Therefore, these findings are consistent with beneficial reversal of dominance, showing
106 that resistant *Ace* alleles persist at intermediate frequencies under temporally fluctuating
107 selection.

Figure 1

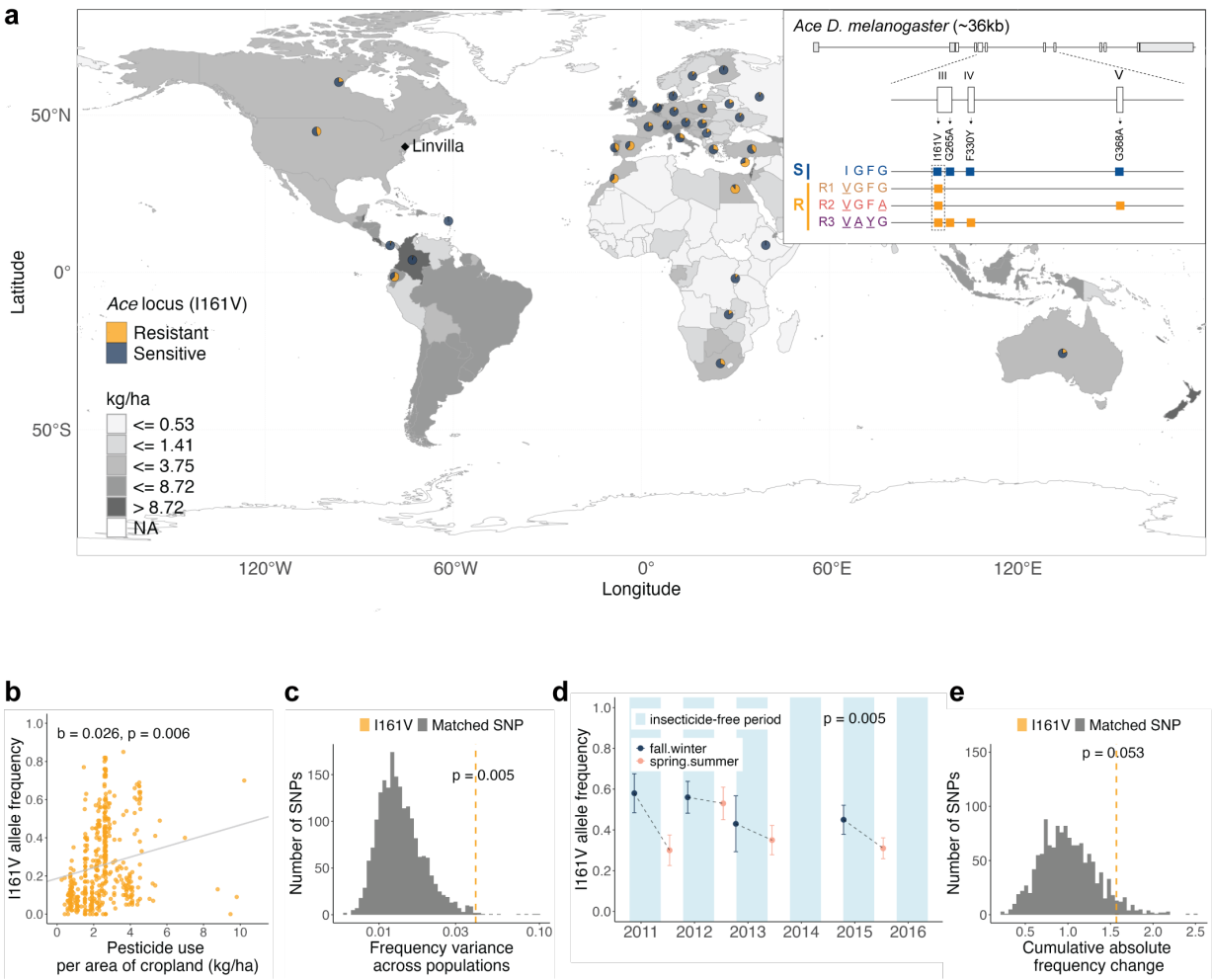

Figure 1. Organophosphate-resistant *Ace* alleles persist at intermediate frequencies in natural *Drosophila melanogaster* populations and respond to spatially and temporally fluctuating insecticide selection. a, Allele frequency map of I161V (pie charts), a marker of organophosphate-resistant *Ace* alleles, overlaid on insecticide use intensity (shading). Inset shows common resistant *Ace* alleles with three different resistance haplotypes (R1: VGFG, R2: VGFA, R3: VAYG) in *D. melanogaster* (See also **Extended Data Fig. 1** for frequencies of resistant haplotypes in DGRP and LNPA panels of fully sequenced inbred lines). **b,** I161V frequency increases with increased pesticide use (linear mixed-effect model). **c,** I161V shows higher variance in frequency compared to matched control SNPs across populations (orange dashed line indicates I161V). **d,** Seasonal changes in I161V frequency at Linvilla Orchards showing decline from fall (dark blue) to spring (pink) samples during insecticide-free periods (turquoise, mid-fall to mid-spring) (generalized linear model, mean ± s.e.m.). **e,** Cumulative frequency changes at Linvilla Orchards samples show elevated allele frequency fluctuations of I161V compared to matched control SNPs (orange dashed line indicates I161V).

110 **Lab experiments reveal dominant benefits and recessive (or co-dominant) costs of resistant**
111 ***Ace* alleles for fitness-associated phenotypes**

112 We then examined whether the resistant *Ace* alleles exhibit beneficial reversal of dominance for
113 fitness associated phenotypes relevant to organophosphate-rich and -free environments. In
114 organophosphate-rich environments, resistance is primarily under selection and the resistant *Ace*
115 alleles should be beneficial because the resistance mutations alter the shape of AChE's active site
116 to prevent pesticide binding[22]. In organophosphate-free environments, life history traits are
117 primarily under selection and the resistant *Ace* alleles should be deleterious because the
118 resistance mutations impair AChE activity and stability[24]. Following Wright's theory of
119 dominance, the resistant alleles should be dominant in organophosphate-rich environments
120 where sensitive alleles become loss-of-function, and recessive in organophosphate-free
121 environments where they themselves become loss-of-function[20] (**Fig. 2a,b**). The underlying basis
122 of this mechanism is that even one copy of the functional allele in each favored environment
123 should provide sufficient gene activity to carry out the required function.

124 To test these predictions, we used the LNPA panel of inbred lines (**Extended Data Fig.**
125 **1a,b**) to generate recombinant populations with homozygous sensitive, homozygous resistant,
126 and heterozygous genotypes for each resistant allele (S: IGFG, R1: VGFG, R2: VGFA, R3:
127 VAYG), an approach[28] that controls for the genomic background, and then measured resistance
128 to the organophosphate insecticide malathion and two key life history traits, viability (egg to
129 adult survival) and fecundity (number of eggs laid by gravid females) (see **Methods** for details).
130 For malathion resistance, the R2 and R3 alleles significantly increased LD_{50} (dose causing 50%
131 egg-to-adult mortality) by ~5.8x and ~7.8x respectively ($p < 0.001$), and were strongly dominant
132 over the sensitive S allele, with dominance *h* of 0.78 and 0.77 for R2 and R3, respectively (p <

133 0.001 for $h > 0.5$ in both cases). The R1 allele showed no significant resistance ($p = 0.646$) with
134 inconclusive dominance effects ($p = 0.751$) (**Fig. 2, Extended Data Fig. 2, Extended Data**
135 **Table 1**). For viability and fecundity, all homozygous resistant genotypes exhibited lower
136 phenotypic fitness values compared to the homozygous sensitive genotype, for either or both of
137 them, with viability reductions ranging from 12.4% to 16.9% (all $p < 0.001$) and fecundity
138 reductions from 16.2% (R2R2, $p = 0.37$) to 46.8% (R3R3, $p < 0.001$). The costs driven by the
139 three resistant alleles were either significantly recessive for at least one of the phenotypes for the
140 strongest resistance alleles R2 and R3 (viability R2: $h = 0.17$, $p = 0.027$, fecundity R3: $h = -0.02$,
141 $p = 0.001$), or indistinguishable from codominance for R1 (**Fig. 2g-l, Extended Data Tables 2-**
142 **3**). Therefore, these findings support the beneficial reversal of dominance of the resistant *Ace*
143 alleles for key fitness associated phenotypes in organophosphate-rich and -free environments.

Figure 2

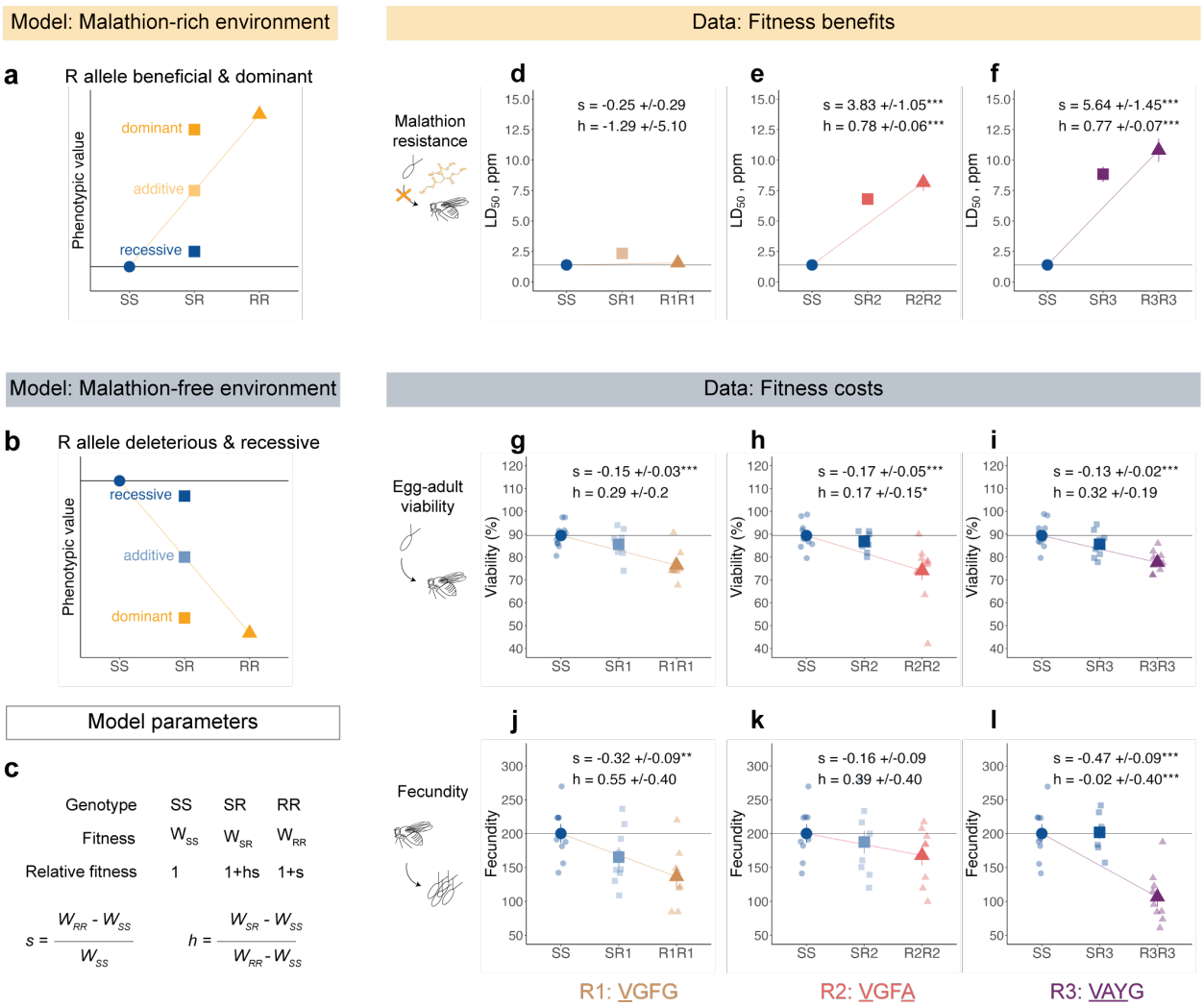

Figure 2. Beneficial reversal of dominance of organophosphate-resistant *Ace* alleles for fitness-associated phenotypes relevant to malathion-rich and malathion-free environments. **a-b**, Under the beneficial dominance reversal, R alleles should be beneficial and partially or completely dominant in malathion-rich environments ($W_{SR} > (W_{SS}+W_{RR})/2$, orange), and deleterious and partially or completely recessive in malathion-free environments ($W_{SR} < (W_{SS}+W_{RR})/2$, blue). **c,** Selection (s) and dominance (h) coefficients for each fitness-associated phenotype are estimated based on the viability selection model. If s>1, the resistant R *Ace* allele is beneficial; if s<1, it is deleterious. If h=1, the resistant R *Ace* allele is dominant to the sensitive S allele; if h=0, the reverse is true. **d-l**, Comparison of malathion LD_{50} (**d,e,f**), egg-adult viability (n=10 technical replicates, 50 eggs/replicate) (**g,h,i**), and fecundity (n=8–10 technical replicates, 5 females/bottle/3 days) (**j,k,l**) among *Ace* genotypes. Malathion LD_{50} was calculated from a four-parameter logistic model fitted to egg-adult viability measurements on media with a range of malathion concentrations (n=2 technical replicates, 50 eggs/replicate, see **Extended Data Fig. 2**). Egg-adult viability and fecundity data were analyzed with logistic and linear regression models.

145 **Field mesocosm experiments reveal dominant benefits and recessive costs of resistant *Ace***
146 **alleles for fitness**

147 We next tested whether beneficial reversal of dominance of the resistant *Ace* alleles drives
148 evolutionary responses to fluctuating insecticide selection in semi-natural conditions and
149 examined its genomic consequences. Given the dominant benefits and recessive costs observed
150 in the laboratory experiments, we predicted a rapid increase in the frequency of the resistant *Ace*
151 alleles and in the level of overall resistance at insecticide concentrations similar to the LD_{50} of
152 the sensitive homozygous genotype. We also predicted a frequency-dependent decline of the
153 resistant *Ace* alleles in the absence of insecticide because recessive costs become exposed in
154 resistant homozygotes when the resistant *Ace* alleles are at high frequencies. For the genomic
155 consequences, we expected that large-amplitude fluctuations of the resistant *Ace* alleles due to
156 fluctuating insecticide selection would drive significant effects on linked genomic variation, as
157 theoretical models suggest[29]. These effects on linked sites should extend across large genomic
158 distances, with their magnitude scaling with the rate of adaptive allele frequency shifts[30].

159 To test these predictions, we conducted a field mesocosm experiment to track the
160 evolutionary dynamics of the resistant *Ace* alleles under controlled seasonal insecticide selection
161 (**Fig. 3a,** see **Methods**). Using an experimental orchard in Pennsylvania, we established 20
162 replicate *D. melanogaster* populations derived from a baseline population constructed from the
163 LNPA panel of inbred lines on June 21, 2021 (**Extended Data Fig. 1**). These lines were outbred
164 for 4 generations in large indoor cages before ~1000 males and females were used to seed each
165 outdoor cage (see **Methods**). After ~4 weeks of untreated propagation, we divided the
166 populations into ten malathion-treated and ten untreated outdoor cages. To mimic natural
167 insecticide exposure, we applied stepwise increasing concentrations of commercial malathion in

168 the growth media of the treated populations (1.5–2.5 ppm from July 21 to August 24, followed
169 by 7.5 ppm until September 6, 2021), exerting strong selection for resistant *Ace* alleles based on
170 our lab LD_{50} measurements (**Extended Data Fig. 2**). Following insecticide removal, all
171 populations were maintained without malathion through December 22, 2021. Throughout the
172 experiment, we tracked population dynamics, malathion resistance by estimating LD_{50}, as well as
173 trajectories of resistant *Ace* alleles and linked sites in response to fluctuating malathion treatment
174 at eight timepoints (~every one to two generations) (see **Methods**).

175 Surprisingly, the malathion treatment did not alter the seasonal population dynamics in
176 the malathion-treated cages (**Fig. 3a**). In all cages, population sizes increased through the
177 summer months until reaching maximum size and then slowly declined in late Fall as abiotic
178 conditions worsened. This suggests that population size in all cages is primarily limited by high
179 levels of pre-adult mortality, potentially masking the additional mortality imposed by malathion.

180 Consistent with our predictions, the frequency of the resistant *Ace* alleles increased
181 rapidly in the malathion-treated cages, followed by a frequency-dependent decline after
182 insecticide removal. By tracking the resistant *Ace* alleles, we found that the R2 and R3 allele
183 frequencies increased during malathion selection (R2: $t = 13.93$, $p < 0.001$; R3: $t = 27.59$, $p <$
184 0.001) (**Fig. 3b**), with the speed of change consistent with the selection coefficients (*hs*) on the
185 order of 150-200% per generation. In contrast, the R1 allele showed no significant increase
186 during treatment, consistent with its lack of detectable malathion resistance in lab assays (**Fig.**
187 **3b, Fig. 2d**). After insecticide removal, only the most common resistant allele (R3) declined ($t =$
188 -5.18, $p < 0.001$), which reflects fitness costs that became evident at high frequencies (**Fig. 3b,**
189 **Extended Data Table 5**).

190 To understand how these allele frequency changes influenced population-level resistance,
191 we tracked malathion resistance throughout the experiment. The frequency increase of the
192 resistant *Ace* alleles coincided with a rapid rise in malathion resistance, with LD_{50} increasing
193 from ~2.2 ppm at the start of treatment to ~12.6 ppm ($t = 24.26$, $p < 0.001$) (**Fig. 3d, Extended**
194 **Data Fig. 3)**. Resistance subsequently declined to ~10.6 ppm after malathion removal ($t = -3.96$,
195 $p = 0.001$), consistent with fitness costs in the absence of selection (**Fig. 3d, Extended Data Fig.**
196 **3, Extended Data Table 4.1)**. To assess the contribution of the *Ace* locus in the evolution of
197 resistance, we applied a viability selection model parametrized by lab-measured genotype
198 viabilities (see **Methods**). This model closely recapitulated both allele frequency trajectories and
199 resistance evolution, strongly suggesting that *Ace* is the major-effect locus driving rapid
200 evolution of resistance to malathion selection (**Extended Data Fig. 4**).
201 In the absence of insecticide selection in the untreated cages, the resistant *Ace* allele
202 frequencies remained stable supporting the prediction that their costs are hidden in
203 heterozygosity (**Fig. 3c**). None of the resistant *Ace* alleles exhibited significant frequency
204 changes (**Fig. 3c, Extended Data Table 6**), suggesting low selection coefficients (s) or
205 dominance parameters (h) in the absence of malathion. Consistently, LD_{50} values remained low
206 and unchanged throughout the experiment (~2.2 ppm, $t = 1.07$, $p = 0.288$) (**Fig. 3d, Extended**
207 **Data Fig. 3, Extended Data Table 4.2**), indicating that overall resistance levels were unaffected
208 in the untreated populations.
209 To further obtain bounds on evolutionary parameters for the resistant *Ace* alleles in
210 organophosphate-free conditions, we fit the allele frequency data of the treated and untreated
211 cages to a viability selection model where all resistant alleles share the same fitness cost (see
212 **Methods**). The model that fit both datasets best had low cost ($s \sim 2.5$ to 5%) and low dominance

213 values ($h < 0.38$) (**Fig. 3f**). At higher values of h, there is no single selection coefficient that can
214 explain the patterns of allele frequency change for both treated and untreated cages, and the
215 likelihood of the data is higher the closer h is to zero. This analysis confirmed our prediction that
216 the fitness cost of the resistant *Ace* alleles is recessive in semi-natural conditions.

Figure 3

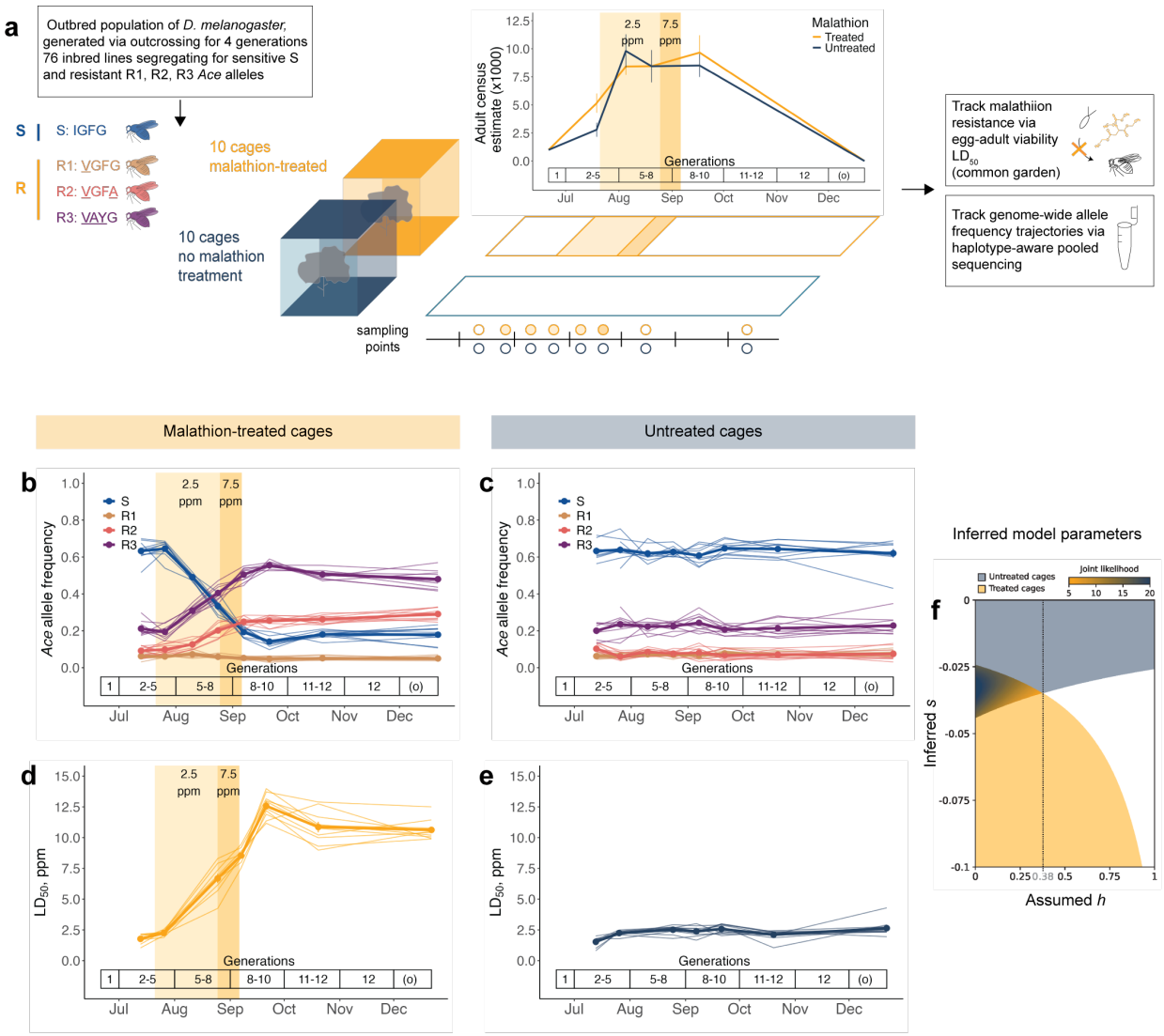

217

Figure 3. Beneficial reversal of dominance of resistant *Ace* alleles for fitness in an ecologically realistic environment. a, Twenty field mesocosm cages were seeded with an outbred population of *D. melanogaster* generated via outcrossing for 4 generations 76 inbred lines carrying the sensitive S and resistant R1, R2, and R3 alleles. Ten cages received a malathion pulse after the initial population establishment. Eight timepoints were sampled to track the evolution of malathion resistance and genome-wide allele in the treated and untreated populations. Malathion did not affect estimated adult fly population sizes (mean ± s.e.m.) in treated populations. **b-c,** Trajectories of *Ace* alleles in treated (**b**) and untreated (**c**) populations. In treated populations, the malathion pulse led to a significant increase in the frequency of the resistant R2 and R3 alleles, followed by a decline in the frequency of R3. *Ace* allele frequencies remained stable in the untreated populations. Light lines/points show individual allele trajectories, dark lines/points represent the mean ± s.e.m. (n = 10 populations per treatment group). **d-e,** The malathion pulse led to a significant increase and subsequent decline of resistance (LD_{50}, ppm) in the treated populations while resistance remained stable in the untreated populations. For LD_{50} calculations see **Methods** and **Extended Data Fig. 3**. (**continued on next page**)

Figure 3 (continued). Light lines/points show individual populations (orange, treated; blue, untreated), dark lines/points represent mean ± s.e.m. (n=10 populations per treatment group).**f,** Inferred selection (s) and dominance (h) coefficients from changes in the resistant *Ace* allele frequency. The colored ranges show the selection coefficients corresponding to the 0.95 confidence intervals of the slope distribution, obtained by bootstrapping cages within each treatment group. The overlap between the orange (treated cages) and dark blue (untreated cages) restricts the possible values of *s* and *h*. Within that overlap, lower values of *h* better explain both sets of data, as shown by higher values of the joint likelihood calculated from the bootstrap distributions (see **Methods**). All results of statistical tests can be found in **Extended Data Tables 4-6**.

Fluctuating insecticide selection generates chromosome-scale genomic perturbations at sites linked to the resistant *Ace* alleles

We then examined the genomic consequences of rapid frequency fluctuations at the *Ace* locus on linked genetic regions. Our experimental design presented us with a rare opportunity to study these effects directly because the linkage patterns of genome-wide SNPs with the *Ace* alleles at the beginning of the experiment are known from the inbred line genotypes. To characterize forward and reverse sweeps driven by the R2 and R3 alleles during and after malathion treatment, respectively, we used a two-step approach (see **Methods**). First, we employed quasibinomial logistic regression to estimate genome-wide allele frequency changes during malathion treatment (July 26 to September 21, 2021) and post-treatment (September 21 to December 22, 2021). Next, we quantified changes in allele frequencies in SNPs tightly linked to the sweeping R2 and R3 alleles across the genome (r2 > 0.03 and frequency > 60% in resistant lines, *Ace*-linked) and those that were largely unlinked (r2 < 0.01, control).

During malathion treatment, we observed a chromosome-wide forward sweep in the malathion-treated cages driven by the R2 and R3 resistant alleles (**Fig. 4a**). The sweep extended across the chromosome arms 3R (~4-17Mbp), including the *Ace* locus (9.6Mb), and 3L (~5-19Mbp), with *Ace*-linked sites showing consistently elevated effect sizes above control sites. The sweep's width is consistent with the extremely rapid rise of the *Ace* alleles over 2-4 generations

237 and the maximum recombination rate of ~5cM/Mbp in *D. melanogaster*, implying the effects
238 conservatively extending over a region of ~5-10 Mbp. Our analysis also indicated the presence
239 of two additional loci potentially responding to malathion selection. On chromosome arm 3L
240 (~19.5Mb), control sites showed a strong directional perturbation while *Ace*-linked sites
241 uniformly decreased in frequency, suggesting interference from another adaptive locus with the
242 *Ace* sweep (**Fig. 4a,** asterisk**)**. A similar pattern was observed on chromosome arm 2R, where
243 both *Ace*-linked and control sites showed comparable frequency perturbations, indicating a
244 second putative locus under selection (**Fig. 4a** asterisk). The study of these additional adaptive
245 loci to malathion treatment is beyond the scope of this work. As expected, in the untreated cages
246 where the frequencies of the R2 and R3 alleles remained stable (**Fig. 3d**), *Ace*-linked sites
247 showed no elevated frequency changes compared to the control sites (**Fig. 4b**).
248 After malathion treatment ceased and selection reversed, we detected an ~5Mbp reverse
249 sweep driven by the R2 and R3 alleles in the malathion-treated cages (**Fig. 4c**). Individual SNPs
250 within 1Mbp of the *Ace* locus demonstrated a strong reversal effect, in which sites that increased
251 in frequency during treatment tended to decrease afterwards, with this reversal being
252 significantly stronger for *Ace*-linked compared to control sites (**Fig. 4e**). As expected, in the
253 untreated populations, *Ace*-linked sites showed neither significant median frequency changes
254 (**Fig. 4d**) nor the reversal behavior (**Fig. 4f**). Notably, recombination through the course of the
255 experiment degraded the initial haplotype structure, suggesting the true extent of the reverse
256 sweep may exceed 5 Mbp. Together, these findings confirmed our predictions that large-
257 amplitude frequency fluctuations of adaptive alleles under temporally varying selection can drive
258 significant effects on linked genomic variation.

Figure 4

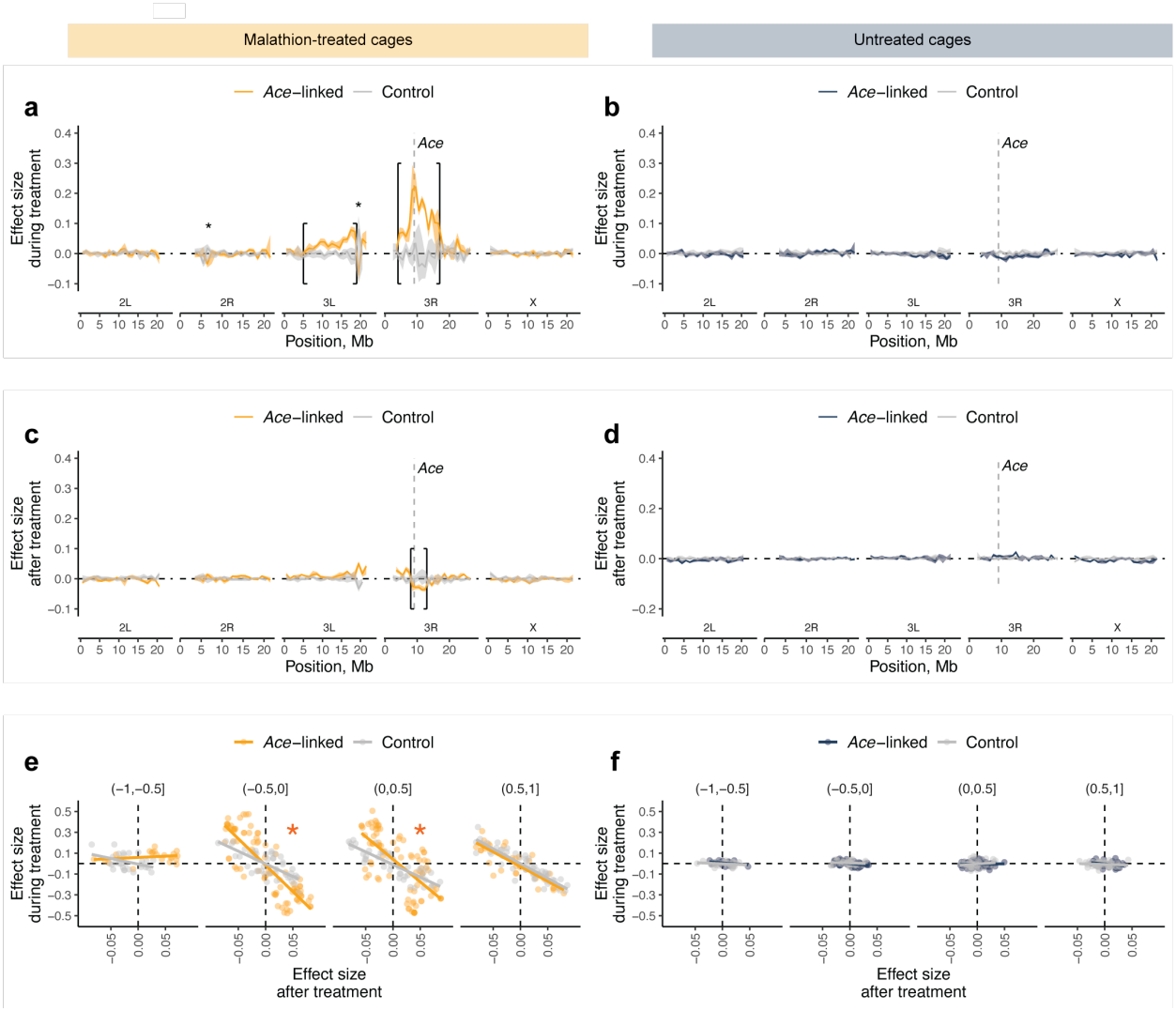

Figure 4. Strong fluctuating selection of resistant *Ace* alleles caused chromosome-scale forward sweep during malathion treatment and reverse sweep after treatment. **a-d**, Effect sizes (median allele frequency changes) for *Ace*-linked (orange/blue) and unlinked control (grey) SNPs in 1Mbp windows across the genome were estimated using quasibinomial logistic regression (see **Methods**). Changes during malathion treatment in treated (**a**) and untreated (**b**) populations. Changes after treatment cessation in treated (**c**) and untreated (**d**) populations. The brackets represent the inferred width of the sweep. Stars indicate additional adaptive loci to malathion treatment. **e-f**, Comparison of effect size for *Ace*-linked (orange/blue) and unlinked control (grey) SNPs during (y-axis) and after malathion treatment (x-axis) in malathion-treated (**e**) and untreated (**f**) populations within 1Mb from *Ace*. Each panel shows SNPs grouped by their distance from *Ace* (in Mb): [-1, -0.5], [-0.5, 0], [0, 0.5], and [0.5, 1]. In panel **e**, red stars indicate regions where the regression slopes significantly differ between *Ace*-linked and unlinked control SNPs.

Discussion

Our study provides compelling empirical evidence for beneficial dominance reversal maintaining a large-effect resistance polymorphism at the *Ace* locus under temporally fluctuating insecticide selection in *D. melanogaster*. Previous studies have suggested the presence of beneficial reversal of dominance of resistant *Ace* alleles in *D. melanogaster* and other resistant insect populations based on the extension of Wright's physiological theory[20], enzymatic studies[22,24], and analysis of fitness-associated phenotypes[19]. While these approaches can provide insights into the functional effects of resistance mutations, they do not necessarily predict organismal and fitness consequences[31]. For example, our results with the R1 allele illustrate this limitation - while enzymatic studies predicted it would confer similar levels of resistance as the R2 allele to malaoxon (the active breakdown product of malathion)[22], we found a very small resistance benefit to malathion at the organismal and fitness levels. The novelty of our work with the *Ace* locus in *D. melanogaster* lies in combining laboratory assays, field mesocosm experiments with insecticide manipulation, and mathematical modeling to directly measure selection and dominance effects on the organismal level and on fitness in semi-natural conditions.

The beneficial dominance reversal we observed at the *Ace* locus suggests this mechanism may be widespread in maintaining functional genetic variation at large-effect loci under temporally fluctuating selection. Indeed, a growing body of literature indicates that beneficial reversal of dominance acts as a common mechanism for maintaining large-effect genetic variation across different forms of antagonistic selection between environments (e.g., fitness components, sexes, or niches/environments)[10,11]. For example, one allele of the large-effect *RXFP2* locus in Soay sheep has a dominant beneficial effect on male mating success but a recessive deleterious effect on male survival[32]. Similarly, the late maturation allele of the large-

284 effect *VGLL3* locus in Atlantic salmon is partially dominant and likely beneficial in females, yet
285 recessive and likely deleterious in males[33]. In the context of temporally fluctuating selection,
286 large-effect loci coding for protein polymorphisms (e.g., enzymes, transcription factors) that are
287 specialized for alternative contexts/substrates may commonly display beneficial reversal of
288 dominance, as environmental shifts render these variants functionally impaired in their unfavored
289 conditions. This pattern follows naturally from Wright's physiological theory of dominance[12],
290 which predicts that the loss of protein function in alternative environments leads to the shifting
291 identity of the recessive, deleterious allele[10,12].

292 Finally, our study examined the genomic consequences of beneficial reversal of
293 dominance at the *Ace* locus under temporally fluctuating selection. Our field mesocosm
294 experiment revealed substantial genomic effects, with the rapid frequency changes at the *Ace*
295 locus driving both a chromosome-wide forward sweep during malathion treatment and a reverse
296 sweep after treatment removal. These findings provide empirical validation of theoretical
297 predictions that beneficial dominance reversal of large-effect alleles can generate large-
298 amplitude frequency fluctuations with significant effects on linked genetic variation[2,29]. Given
299 that the *D. melanogaster* genome contains a fair number (tens to hundreds) of large-effect alleles
300 displaying large frequency shifts due to fluctuating selection[5,6] and the likelihood that this is the
301 case for many other species[34,35], fluctuating selection at large-effect loci could act as a major
302 force shaping levels of genetic variation in natural populations[29].

Acknowledgements This project was supported by grants from the National Institute of General Medical Sciences of the National Institutes of Health (Award number 1K99GM143455-01 to M.K, Grant 5R01GM100366-08 and 5R01GM137430-02 to P.S., Award Number 5R35GM118165-07 to D.A.P), the Sarah Hotchkis Ketterer Graduate Fellowship from Stanford University (to A.S.L.), the National Science Foundation (Grant PRFB 2109407 to M.C.B.), and the Stanford Biology Summer Undergraduate Research Program (to Z.K.M. and A.H.). The authors thank Marcus Feldman for helpful discussions and assistance with modeling *Ace* allele frequency evolution, Danae Papadopetraki for assistance with statistical analyses of the phenotypic and genomic data, Axel Wiberg for feedback on statistical analyses of the genomic data, Emily Behrman for feedback on the day degree model for generation estimation, Jessica Rhodes for helpful discussions and assistance with statistical analyses of the DEST data, and Anastasia Andreeva for assistance with phenotyping. The authors are very grateful to Jean Villa, Jessica Rhodes, Meike Wittmann, Noah Whiteman, and Marcus Feldman for feedback that improved the earlier versions of the manuscript.

Author Contributions M.K was responsible for conceptualization, investigation, formal analysis, writing original draft, writing-review and editing, visualization, and funding acquisition; A.L. was responsible for formal analysis, visualization, and writing-review and editing; M.B. was responsible for formal analysis and investigation; E.L. was responsible for formal analysis, visualization, and writing-review and editing; S.G. was responsible for formal analysis; A.H., CT, and Z.K.M. were responsible for investigation; P.S. and D.A.P. jointly supervised the research. P.S. was responsible for conceptualization, investigation, formal analysis, writing-review and editing, and funding acquisition. D.A.P. was responsible for conceptualization, investigation, formal analysis, writing-review and editing, and funding acquisition.

327 **Methods**

328

329 **Population genomic analysis for variation of organophosphate-resistant *Ace* alleles across**

330 **space and time**

331 We first conducted a literature review to compile all known naturally segregating target site

332 resistance mutations in the acetylcholinesterase (*Ace* gene) protein of *D. melanogaster* that

333 confer resistance to organophosphates. Mutero and colleagues in 1994[36] first identified the

334 resistance mutations F115S, I199V, I199T, G303A and F368Y, and numbered them based on the

335 precursor acetylcholinesterase (AChE) protein. Menozzi and colleagues in 2004[22] identified

336 combinations of the resistance mutations I161(199)V, G265(303)A, F330(368)Y and

337 G368(406)A in worldwide organophosphate-resistant *D. melanogaster* strains and numbered

338 them based on the mature AChE protein (numbers in the brackets refer to the precursor AChE

339 protein). They did not identify the resistance mutation F77(115)S. At position 77, the mutation

340 TTC to T**C**C changes phenylalanine to serine (Chr3R: 9,070,101, v5.39). At position 161, the

341 mutation ATC to **G**TC changes the isoleucine to valine (Chr3R:9,069,721, v5.39). At position

342 265, the mutation GGC to G**C**C changes the glycine to alanine (Chr3R:9,069,408 , v5.39). At

343 position 330, the mutation TTT to T**A**T changes the phenylalanine to tyrosine (Chr3R:9,069,054

344 , v5.39). At position 368, the mutation GGC to G**C**C/G**CT** changes the glycine to alanine

345 (Chr3R: 9,063,921 , v5.39). The AChE protein's numbering changed between the studies after its

346 crystallization in 2000, which defined the N-terminal signal peptide and the C-terminal

347 sequence[37]. The mutation G368A was missanotated in the study of adaptation of *D.*

348 *melanogaster* to organophosphate insecticides by Karasov and colleagues[23].

349

350 <u>Organophosphate-resistant *Ace* alleles in DGRP and LNPA inbred lines</u>

351 We characterized the presence of organophosphate-resistant *Ace* alleles in two fully
352 sequenced inbred line panels, the Drosophila Genetic Reference Panel (DGRP) and our LNPA
353 panel of inbred lines. The DGRP panel consists of 205 inbred lines derived from wild-caught
354 females collected at the Raleigh, North Carolina Farmers Market in 2003[25]. The LNPA panel
355 consists of 76 inbred lines derived from wild-caught individuals collected in Spring and Fall
356 from Linvilla Orchards, Media PA USA[5]. Both panels contain the two common resistant *Ace*
357 alleles (Ace-R1: VGFG and Ace-R3: VAYG) at high frequency, the sensitive *Ace* allele (Ace-S:
358 IGFG), and other rare resistant alleles. The LNPA panel also contains the resistant *Ace* allele
359 Ace-R2: VGFA at high frequency. We used the LNPA panel for our lab and field mesocosm
360 experiments.
361
362 Spatial and seasonal variation of organophosphate-resistant *Ace* alleles in natural *Drosophila*
363 *melanogaster* populations
364 To examine the spatial variation of the I161V polymorphism, a marker of common
365 organophosphate-resistant *Ace* alleles (Ace-R1: VGFG, Ace-R2: VGFA, Ace-R3: VAYG), we
366 first analyzed the relationship between country-level pesticide use and I161V frequency in
367 *Drosophila melanogaster* populations. We obtained pesticide use data from the Food and
368 Agriculture Organization (FAO) FAOSTAT database[27], which provides country-level estimates
369 of pesticide use per area of cropland. For population genomic data, we used the Drosophila
370 Evolution over Space and Time (DEST) database, which contains pooled genome-wide allele
371 frequency estimates from 753 population samples of *D. melanogaster* collected worldwide. For
372 our analyses, we included pesticide use data and genomic data for the period of 2000-2022.

To visualize the spatial distribution of insecticide use and frequency of the I161V polymorphism across locations, we created a choropleth map where countries are shaded based on their pesticide use per cropland area, with pie charts indicating the frequency of the resistant (I161V) and sensitive alleles at sampled locations. For each location, we calculated median allele frequencies across available samples for the period 2000-2022. To test whether insecticide use predicts the frequency of the resistance allele I161V, we fitted a linear mixed effects model using the lmer() function in the R package lme4 (version 1.1.33). The model included I161V frequency as the response variable and insecticide use per cropland area as a fixed effect. We included a random effect for cities.

In addition, to further test whether I161V shows evidence of spatial selection rather than drift, we compared its variance across samples collected in spring to matched control SNPs. We selected control SNPs based on three criteria: (1) located within 2Mb but at least 100kb away from *Ace* to avoid linked SNPs, (2) within the ln(3R)K cosmopolitan inversion to match inversion status, and (3) average frequency across samples within 4% of the median frequency of the I161V resistance mutation. We used the cumulative distribution function (CDF) to quantify how extreme the I161V variance was compared to the control SNPs.

To examine the temporal variation of the I161V polymorphism, we first tested two hypotheses: (1) whether the frequency of the resistant allele decreases during winter months when insecticide pressure is relaxed, potentially due to fitness costs, and (2) whether the frequency of the resistant allele increases during the growing seasons when insecticides are applied. We analyzed time series data from Linvilla Orchards, a non-organic orchard in Pennsylvania, USA. Samples were collected near apple trees from 2009 to 2015, with paired spring and fall collections each year, allowing us to test both hypotheses. To account for

396 sampling variance in pooled sequencing data, we calculated the effective number of
397 chromosomes sampled (Nc) following Machado et al. (2016), where Nc = (1/N + 1/R)^(-1), with
398 N being the number of chromosomes in the pool (2 × number of flies) and R the read depth at the
399 site. We then tested for systematic seasonal changes using generalized linear models (GLM) with
400 binomial error structure. The models used the number of resistant and susceptible alleles
401 (weighted by Nc) as the response variable and season as a categorical predictor. For the winter
402 decline hypothesis, we paired each fall sample with the following spring sample. For the summer
403 increase hypothesis, we paired each spring sample with the following fall sample from the same
404 year. This approach allowed us to directly test for consistent directional changes in allele
405 frequencies across seasons while accounting for both biological and technical sources of variance
406 in the data.

407 Finally, to test whether the temporal dynamics of I161V reflect selection rather than drift,
408 we compared its frequency fluctuations to those of matched control SNPs at Linvilla. To
409 quantify temporal variation, we calculated the cumulative absolute change in I161V allele
410 frequency over time as the sum of frequency differences between consecutive timepoints. This
411 metric captures the total magnitude of frequency changes, regardless of direction. We selected
412 control SNPs that had similar starting conditions as I161V, with initial frequencies matching the
413 I161V frequency (0.42) at the first Linvilla timepoint within ±4%. To ensure a valid comparison,
414 control SNPs were selected from within the same genomic region and inversion status as I161V,
415 while excluding potentially linked sites (same criteria as for the spatial analysis). We then used
416 the cumulative distribution function to assess whether I161V's temporal variation was
417 significantly greater than that observed in the matched control SNPs, which would suggest that
418 its frequency changes are driven by seasonal selection rather than drift.

419

420 **Laboratory experiments to estimate the dominance of resistant *Ace* alleles for fitness-**
421 **associated phenotypes in the presence and absence of malathion**

422 To assess whether the dominance of each resistant *Ace* allele (Ace-R1: VGFG, Ace-R2: VGFA,
423 Ace-R3: VAYG) over their sensitive counterpart (Ace-S: IGFG) reverses for fitness-associated
424 phenotypes that are primarily under selection in organophosphate-rich and -free environments,
425 we first used our LNPA panel of inbred lines to generate recombinant populations with
426 homozygous sensitive, homozygous resistant, and heterozygous *Ace* genotypes for each *Ace*
427 allele. This step was meant to bring potential deleterious, recessive mutations in the inbred lines
428 into heterozygosity. We then measured malathion resistance, viability and fecundity in
429 homozygous and heterozygous populations for each *Ace* genotype.

430

431 Generation of recombinant populations with homozygous sensitive, homozygous resistant, and
432 heterozygous *Ace* genotypes

433 To generate recombinant populations for each *Ace* allele, we first intercrossed 2-3 inbred
434 lines with the same *Ace* allele using a round robin cross scheme (e.g., Line_1 SS x Line_2 SS,
435 Line_2 SS x Line_3 SS, Line_3 SS x Line_1 SS) to bring all founders with the same *Ace* allele
436 together (10 non-mated females x 10 males per round robin cross). We then combined 16 F1
437 flies (8 non-mated females and 8 males) from each of the round robin crosses per *Ace* allele to
438 establish the next generation. Subsequently, we maintained the homozygous populations in vials
439 and allowed them to recombine for four generations until we performed the phenotype
440 measurements. We used lines 12LN6-70_(B33), 12LN6-92_(B3), LNPA-3 for the sensitive *Ace*
441 allele (Ace-S: IGFG), lines 12LN6-86_(B29) and LNPA-53 for the R1 resistant *Ace* allele (Ace-

442 R1: VGFG), lines LNPA-14, LNPA-17 and LNPA-87 for the R2 resistant *Ace* allele (Ace-R2:
443 VGFA), and lines 12LN6-45_(B26), 12LN6-82_(B4), and 12LN6-94_(B19) for the R3 resistant
444 *Ace* allele (Ace-R3: VAYG).
445
446 Measurements of fitness-associated phenotypes
447 For all experiments, we first set up breeding cages with ~ 500 4-to-7-day-old flies of
448 homozygous or heterozygous populations for the sensitive and the resistant *Ace* alleles. To
449 generate the heterozygous recombinant populations, we crossed SS non-mated females with
450 homozygous males of each resistant allele (R1R1, R2R2, R3R3).
451 To compare the level of malathion resistance among the different alleles, we measured
452 egg-to-adult viability on diets that ranged in malathion concentration from 0 ppm to 30 ppm. For
453 this, we collected eggs of each population that were laid within a period of 24 hours and then
454 introduced 50 eggs of each population into narrow vials containing approximately 7 ml of
455 *Drosophila* growth media supplemented with the respective malathion concentration. We tested
456 each of the malathion concentrations in duplicate vials. We used commercial malathion of 50%
457 strength (Southern Ag Malathion 50% E.C.) and dissolved it in the *Drosophila* growth media.
458 This medium was kept overnight at 4ºC and used the next day for the assay. We monitored adult
459 eclosion every evening over a period of 10 days until all adult flies had enclosed.
460 To compare viability among the different genotypes, we introduced 50 eggs of each
461 population into narrow vials containing ~7 ml of *Drosophila* growth media. Each of the
462 genotypes were tested in 10 replicate vials. We monitored adult eclosion every evening over a
463 period of 7 days until all adult flies had enclosed.

464 To compare fecundity among the different genotypes, we used density-controlled (~50
465 eggs/vial) adult female progeny of each population. We introduced five 3-day-old females of
466 each genotype in egg-laying bottles fitted with egg-laying caps filled with Drosophila growth
467 media. Each day over a period of 3 days we counted the number of eggs laid. Each of the
468 genotypes were tested in 8-10 replicate egg-laying bottles. The egg-laying caps were examined
469 under a stereoscope where we counted the eggs laid each day over the 3-day period.
470
471 Statistical analysis of fitness-associated phenotypes
472 We assessed fecundity, viability, and malathion resistance for the three genotypes (SS,
473 SR, RR) of each *Ace* allele (R1, R2, R3) using R (version 4.2.2). For fecundity and viability, we
474 fitted linear and logistic regression models, respectively, calculating estimated marginal means
475 and performing pairwise comparisons adjusted for multiple testing using the Benjamini-
476 Hochberg procedure. We then implemented a bootstrap procedure (1,000 resamples) to estimate
477 deviation from additivity, selection coefficient, and dominance coefficient. The deviation from
478 additivity was calculated as W[SR] - (W[SS] + W[RR]) / 2, where W represents fitness
479 (fecundity or viability) for each genotype. The selection coefficient *s* was computed as (W[RR] –
480 W[SS]) / W[SS], indicating the relative fitness of the resistant genotype compared to the
481 sensitive genotype. The dominance coefficient *h* was calculated as (W[SR] – W[SS]) / (W[RR] –
482 W[SS]), measuring the degree to which the heterozygote phenotype is closer to either
483 homozygote. Significance was assessed by testing whether results differed from zero (additivity
484 and selection) or 0.5 (dominance). For malathion resistance, we estimated LD_{50} values for each
485 genotype using four-parameter logistic dose-response models f(x) = c + (d-c) / (1 + e^(b(x-e))),
486 where e is LD_{50}, d (upper limit) = 100%, c (lower limit) = 0%, and b is the relative slope around

487 e. For this, we used the L.4() function in the drc package (version 3.0.1)[38] in R (version 4.2.2)
488 with egg to adult viability at the range of malathion concentrations as the response variable. We
489 then used a bootstrap procedure (1,000 resamples) to compare LD_{50} values between genotypes
490 and calculate the same coefficients, substituting LD_{50} values for W in the formulas. For all
491 analyses, bootstrap resampling was used to calculate confidence intervals and p-values, with
492 significance assessed against null hypotheses of 0 (additivity and selection) and 0.5 (dominance).
493

494 **Field mesocosm experiments to track the evolution of malathion resistance and genome-**
495 **wide allele frequencies in the presence and absence of fluctuating malathion selection**
496

497 Experimental orchard and field mesocosm cages

498 To mimic the natural surroundings and weather conditions that flies are exposed to in nature, we
499 conducted the study in an experimental orchard at the University of Pennsylvania in
500 Philadelphia. The orchard consisted of cleared land with walk-in mesocosm cages (2m x 2m x
501 2m) constructed of fine mesh and built around metal frames (BioQuip PO 1406C). We planted a
502 dwarf peach tree in each mesocosm cage to provide flies with shade. All peaches were removed
503 before ripening to prevent flies from feeding or laying eggs on them. To provide flies with a
504 feeding and breeding substrate, we added 1.5lb aluminum loaf pans with 400ml Drosophila
505 growth media every two days during the experiment. To avoid an overcrowded developmental
506 environment for the eggs, each loaf pan was covered with a screen mesh lid every two days
507 during the experiment, and eggs were allowed to develop until eclosion ceased, at which point
508 adult flies were released into the general population. The loaf pans were placed on a shelving
509 unit oriented away from direct sunlight to protect them from rain and direct sun.

510

511 Establishment of experimental *D. melanogaster* populations in field mesocosm cages

512 To construct the baseline *D. melanogaster* population for the experiment, we crossed the
513 76 fully sequenced LNPA inbred lines from Pennsylvania. We used inbred lines to facilitate the
514 use of haplotype inference to attain high effective sequencing coverage[39]. To initiate the baseline
515 population, we combined 10 females and 10 males from each line into a single breeding cage.
516 After 4 generations of mating and density-controlled rearing in laboratory conditions, we
517 introduced 500 females and 500 males of a single age cohort into each mesocosm cage on June
518 21, 2021.

519

520 Malathion treatment over the course of the experiment

521 A diagram of the experimental design is shown in **Fig. 3a**. In the first step (*Establishment*
522 *phase*: June 21 to July 20, 2021), we established 20 replicate populations in mesocosm cages and
523 allowed them to expand in the absence of interventions. After establishment, the populations
524 were split into ten malathion-treated and ten malathion-untreated populations. To mimic the
525 insecticide exposure of flies in nature, the malathion-treated populations were exposed to
526 malathion in the summer. In nature, insecticides are mainly applied during summer for pest
527 control and their application ceases in the fall[40]. During the malathion treatment phase of the
528 experiment, we sequentially exposed the populations to stepwise increasing concentrations of
529 malathion, from 1.5 (July 21 to July 27, 2021) to 2.5ppm (July 28 to August 24, 2021) and
530 7.5ppm (August 25 to September 6, 2021). We used commercially available malathion grade of
531 50% strength (Southern Ag Malathion 50% E.C.) and dissolved it in the *Drosophila* growth
532 media. We selected malathion doses based on the Malathion 50% E.C. label instructions to

533 control small insect pests in the field and a previous long-term selection experiment for
534 malathion resistance in *D. melanogaster*[41]. The medium supplemented with malathion was
535 cooked once per week and stored at 4˚C until deployed. After the malathion treatment, the
536 experiment lasted until early winter (September 7 to December 22, 2021). Over the course of the
537 experiment, we performed high-resolution temporal sampling (~ bi-weekly sampling during the
538 summer and monthly during the fall) to track evolution of malathion resistance and genome-wide
539 allele frequencies.
540

541 **Tracking population size in the field mesocosms**

542 To make relative comparisons of population sizes between the malathion-treated and untreated
543 cages, we photographed 4 equal-size quadrats of the ceiling in each cage at dusk (approximately
544 2.5% of the ceiling for each quadrat). To count the number of adult flies in each photograph, we
545 designed and validated an algorithm for semi-automated image processing. The number of adult
546 flies in each of the 4 photographs was multiplied by 40 to correct for total surface area and obtain
547 4 population size estimates per cage.
548

549 <u>Statistical analysis of population data</u>

550 To assess the effects of time and malathion treatment on population size, we fitted a linear
551 mixed-effect model with the estimated population size as the response variable. We defined our
552 model to investigate the quadratic relationship of time with population size and to account for the
553 random effects attributable to differences in cages. The regression analysis was performed in R
554 (version 4.2.2) using lme4 (version 1.1.33).
555

556 **Tracking malathion resistance in the field mesocosms**

557 To characterize the rate and direction of the evolution of malathion resistance in the malathion-
558 treated and untreated populations, we repeatedly assayed the evolving populations. Prior to the
559 malathion resistance assay, we collected F1 eggs from each mesocosm cage and transferred them
560 in 2 groups of 200 eggs to bottles with media (i.e., density controlled) in a constant common
561 garden environment (25˚C, 12L:12D, 50% humidity) in the laboratory to distinguish evolution
562 from phenotypic plasticity. We then performed the malathion resistance assay with density and
563 age-controlled individuals from each mesocosm cage in the F2 generation (25˚C, 12L:12D, 50%
564 humidity). The common garden experiment for assaying malathion resistance took place at
565 Stanford University with F1 eggs in bottles with media shipped overnight from the University of
566 Pennsylvania.

567

568 Malathion resistance measurements

569 To characterize the level of malathion resistance in the malathion-treated and untreated
570 populations, we tracked egg to adult survival in the F2 generation on diets that ranged in
571 malathion concentration from 0 ppm to 15 ppm over the course of the experiment. For the
572 collection of F2 eggs, we placed ~ 400 4-to-7-day-old F1 individuals in breeding cages with egg
573 lay caps for 5-7 hours. We then introduced 50 F2 eggs in a narrow vial containing ~7ml of
574 *Drosophila* growth media supplemented with malathion. We tested each of the malathion
575 concentrations in duplicate vials. We used commercial malathion of 50% strength (Southern Ag
576 Malathion 50% E.C.) and dissolved it in the *Drosophila* growth media. This medium was kept
577 overnight at 4ºC and used the next day for the assay. We monitored adult eclosion every evening
578 over a period of 10 days until all adult flies had eclosed.

579

580 Statistical analysis of malathion resistance data

581 To assess the temporal dynamics of malathion resistance in both malathion-treated and untreated
582 cages, we fitted separate linear mixed-effects models using the lmer() function in the R package
583 lme4 (version 1.1.33). The response variable in these models was malathion resistance, measured
584 as the LD_{50} value, the dose that causes 50% egg-to-adult mortality. For the malathion-treated
585 cages, we modeled resistance changes over two distinct time periods: (1) from July 26, 2021, to
586 September 21, 2021, when populations were evolving under malathion treatment, and (2) from
587 September 21, 2021, to December 22, 2021, after malathion treatment had ceased. In contrast,
588 for the malathion-untreated cages, we assessed resistance changes over the full experimental
589 period, from July 26, 2021, to December 22, 2021. To avoid biases, we excluded data from July
590 13, 2021, because the LD_{50} estimate from this time point was underestimated due to a technical
591 error. In each model, we included time point as fixed effect, while a random intercept was
592 included for each cage to account for between-cage variability. The main outcome measure of
593 malathion resistance for each cage at each time point was the mean of 1–2 technical replicate
594 LD_{50} measurements. To estimate LD_{50} for each technical replicate per cage per time point, we
595 fitted four-parameter logistic dose-response models using the L.4() function in the drc package
596 (version 3.0.1) in R (version 4.2.2) with egg to adult viability at the range of malathion
597 concentrations as the response variable.

598

599 **Track genome-wide allele frequencies in the field mesocosms over time**

600

601 To track the trajectories of the resistant and sensitive *Ace* alleles and characterize the extent of
602 the sweep caused by the *Ace* alleles, we tracked genome-wide allele frequencies of the evolving

603 populations across the experiment using the software tool HAF-pipe. HAF-pipe estimates
604 genome-wide allele frequencies in the evolving populations via inference of known founder
605 haplotypes from low-coverage pooled sequencing data [39]. As part of our experimental design, we
606 performed whole-genome, low-coverage pooled sequencing of 100 randomly selected F1
607 females from each of the 20 evolving populations at eight time points through the experiment. To
608 measure biological and technical variation, we performed whole-genome, low-coverage pooled
609 sequencing of different sets of 100 randomly selected F1 females from the 20 evolving
610 populations at two time points collected at Stanford (biological replicates) and of same samples
611 of 100 randomly selected F1 females but processed independently (technical replicates). Last, to
612 evaluate the accuracy of HAF-pipe, we performed whole-genome, high-coverage pooled
613 sequencing of four biological replicate samples from the baseline population and for the evolving
614 populations at an early and a late time point. The data for the untreated cages were also used for
615 a recent independent study from Bitter and colleagues [6].
616
617 Sample collection, DNA extraction, library preparation, and sequencing
618 We collected samples from each population approximately every two generations during
619 the summer phase and every generation during the fall phase. To collect the samples, we placed a
620 new loaf pan with Drosophila growth media in each mesocosm cage one day before collection.
621 The next day, we transferred five groups of 200 F1 eggs to bottles with media, where we
622 controlled the density and maintained them in a constant laboratory environment of 25°C,
623 12L:12D, and 50% humidity. Three bottles with F1 eggs were kept at UPenn and two bottles
624 with F1 eggs were shipped overnight to Stanford. At Stanford, F1 adults were allowed to lay
625 eggs, and 200 F2 eggs were placed in vials for density control. For both the F1 and F2

626 generation, we harvested 4-to-7-day-old individuals after eclosion and preserved them in 100%
627 ethanol in 1.5ml vials at -20°C until further processing.
628 For each sample, we prepared genomic DNA from pools of 100 ethanol-preserved
629 females. We first submerged the samples twice in a rehydration buffer (400 mM NaCl, 20 mM
630 Tris-HCl pH 8.0, 30 mM EDTA) for 15 min at room temperature and then isolated genomic
631 DNA using the Monarch Genomic DNA purification kit (Cat No. 3010L, New England Biolabs).
632 The manufacturer's protocol was modified to include a step for tissue homogenization with two
633 3mm glass beads (Cat No. 11-312C, Fisher Scientific) in a bead beater for five minutes to ensure
634 complete homogenization of the flies so that the genomic DNA from each fly was equally
635 represented in the genomic DNA pool. We quantified the genomic DNA using the Qubit dsDNA
636 BR (Broad-Range) Assay kit (Cat No. Q32853, Life Technologies) on a Qubit
637 spectrophotometer and estimated its purity on a NanoDrop spectrophotometer.
638 We then prepared sequencing libraries using the Illumina DNA prep, (M) Tagmentation
639 kit (Cat No. 20018705, Illumina Inc.) and the Illumina UD Indexes sets (Cat No 20027123,
640 20027214, 20042666, 20042667, Illumina Inc.) for unique dual indexing. We modified the
641 manufacturer's protocol by preparing libraries in 1/5 of the recommended reaction volume to
642 maximize kit efficiency and pooling equimolarly amplified libraries in sets of eight after the
643 library amplification step. After the cleanup, we quantified the pooled libraries using a Qubit
644 spectrophotometer and an Agilent Bioanalyzer. Finally, the pooled libraries were 150bp paired-
645 end sequenced on the NovaSeq 6000 S2 platform at the Sequencing Service Center at the
646 Stanford Genomics Center and on a NovaSeq 6000 SP platform at Admera. All sequences will
647 be deposited in SRA.
648

649 Processing of DNA sequencing data for genome-wide allele frequency estimation

650 We trimmed the raw sequencing reads of adapter sequences and bases with quality score
651 < 20. We then mapped the trimmed reads to the *D. melanogaster* reference genome (v5.39) using
652 bwa and default parameters [42], and aligned reads were deduplicated using Picard tools. We
653 randomly sampled reads from the aligned bams to obtain an equivalent, genome-wide coverage
654 of 8x across all samples. We computed haplotype-derived allele frequency (HAF) estimates
655 using HAF pipe. Briefly, after using an expectation-maximization algorithm to estimate
656 haplotype frequencies in overlapping genomic windows from mapped sequence reads (originally
657 developed by Kessner and colleagues [43]) at each site previously identified as polymorphic in the
658 inbred reference panel, we summed the estimated frequencies of haplotypes carrying the
659 alternate allele to obtain HAFs . We conducted haplotype inference in window sizes that varied
660 proportionally to the expected length of un-recombined haplotype blocks, which varied as a
661 function of the estimated number of generations since the original outbreeding. HAFs were
662 compiled to only include those sites with an average minor allele frequency (MAF) > 0.02 in the
663 baseline population, and present in at least one evolved sample at a MAF > 0.01.

664

665 **Track trajectories of sensitive and resistant *Ace* alleles in the evolving populations over**
666 **time**

667

668 We first estimated the frequency of each of the 76 founder haplotypes in the *Ace* region
669 (Chr3R:9,063,921-9,069,721) in each of the malathion-treated and malathion-untreated
670 populations at each time point, focusing on the founders containing the four known resistance
671 mutations . To obtain an accurate measure of the frequency of each haplotype, we calculated the

672 mean frequency across the 10 overlapping genomic windows that included each site within the
673 region of interest.
674 We then estimated the relative frequency of each *Ace* allele, defined by the combination
675 of the four known resistance mutations, in each population at each time point. Given our
676 knowledge of the resistance mutation combinations for each founder, we computed the relative
677 frequency of each *Ace* allele (Ace-S: IGFG, Ace-R1: VGFG, Ace-R2: VGFA, Ace-R3: VAYG,
678 Ace-R4:IGFA, Ace-R5:IGYG, Ace-R6:VAFG, Ace-R7: VAYA) by summing the frequencies of
679 the haplotype blocks from the 76 founders that shared the same *Ace* allele. For founders
680 heterozygous for the *Ace* alleles, we divided the contributions of their haplotype block evenly
681 between the two corresponding *Ace* allele frequencies. *Ace* alleles with a frequency < 0.01%
682 (Ace-R4:IGFA, Ace-R5:IGYG, Ace-R6:VAFG, Ace-R7: VAYA) in the evolving populations
683 were excluded from further analysis.
684
685 Statistical analysis of *Ace* allele frequency data
686 To assess the temporal dynamics of *Ace* allele frequencies (Ace-S: IGFG, Ace-R1:
687 VGFG, Ace-R2: VGFA, Ace-R3: VAYG), we fitted separate linear mixed-effects models using
688 the lmer() function in the R package lme4 (version 1.1.33). The response variables in these
689 models were the frequencies of each *Ace* allele. For the malathion-treated cages, we modeled *Ace*
690 allele frequency changes over two distinct time periods: (1) from July 26, 2021, to September 21,
691 2021, when populations were evolving under malathion treatment, and (2) from September 21,
692 2021, to December 22, 2021, after malathion treatment had ceased. In contrast, for the
693 malathion-untreated cages, we assessed *Ace* allele frequency changes from the beginning of the
694 treatment to the end of the experiment, from July 26, 2021 to December 22, 2021.
695

Model *Ace* allele frequency evolution

We simulated the evolution of *Ace* allele frequencies and malathion resistance in our mesocosm experiments using a viability selection model[44]. Additionally, based on the changes in *Ace* allele frequencies in malathion-free environments across both sets of cages, we estimated the possible ranges for the fitness costs of and dominance of malathion resistance.

<u>The impact of viability on *Ace* allele frequency dynamics and malathion resistance in the field mesocosm experiment</u>

We investigated whether selection acting on viability recapitulates the allele frequency and malathion resistance dynamics observed in the field. We focused on viability as it is a key fitness-related trait in both malathion-rich and malathion-free environments. Furthermore, we had laboratory measurements of viabilities for *Ace* genotypes across ranges of malathion concentrations, allowing us to parametrize our model and test its predictions.

Within our model, the population frequencies of the *Ace* alleles change only due to selection that acts on viability. We assumed that the effects of other forces (mutation, recombination, and genetic drift) were negligible in comparison over the timescales that we considered (~10 generations). Under these assumptions, the frequency dynamics of the sensitive (f_0) and resistant (f_1, f_2, f_3) *Ace* alleles follow from

$$f_i(t+1) = \frac{f_i(t)\sum_j w_{ij} f_j(t)}{\overline{w}(t)},$$

where t is time measured in generations, w_{ij} is viability of individuals carrying both i and j alleles, and $\underline{w}$ is the mean population viability defined as

$$\overline{w}(t) = \sum_{i,j} f_i(t) f_j(t) w_{ij}.$$

We used laboratory measurements to determine individual viabilities w_{ij} in the absence and presence of malathion (at 2.5 and 7.5 ppm). We used the marginal mean values from the linear model for viability for each genotype and the predicted viability values from the dose-response analysis (see previous section on 'Statistical analysis of fitness-associated phenotypes'). Due to the lack of measurements for heterozygous resistant genotypes, we assumed that combinations of resistant alleles are codominant, i.e. that $w_{12} = 0.5 \cdot w_{11} + 0.5 \cdot w_{22}$; $w_{13} = 0.5 \cdot w_{11} + 0.5 \cdot w_{33}$; $w_{23} = 0.5 \cdot w_{22} + 0.5 \cdot w_{33}$. The initial *Ace* allele frequencies, $f_i(0)$, were estimated as the median values from the first sampling time point (July 13, 2021) for each treatment group.

To estimate *D. melanogaster* generation times at our eight sampling time points, we used a degree-day model based on Behrman and Schmidt[53]. This model assumes *D. melanogaster* requires 112 degree-days to complete one generation, with development occurring between 12°C and 29°C. We calculated daily degree-days as [(daily max. temp. + daily min. temp.) / 2] - 12°C, adjusting temperatures outside the 12-29°C range to these limits. Cumulative degree-days were tracked, with each 112 degree-day accumulation marking a new generation. This allowed us to estimate generations at each sampling time point throughout the experiment.

We then calculated the population resistance R as a weighted sum,

$$R(t) = \sum_{i,j} g_{ij}(t) w_{ij},$$

where $g_{ij}(t)$ are genotype frequencies and w_{ij} are the corresponding viabilities. The initial genotype frequencies were estimated from the initial allele frequencies, assuming Hardy-Weinberg equilibrium:

$$g_{ij}(0) = f_i(0) f_j(0).$$

The consequent genotype frequencies followed from the viability selection model,

742 $$g_{ij}(t) = \begin{cases} \frac{2f_i(t)f_j(t)w_{ij}}{\overline{w}}, i \neq j, \\ \frac{f_i(t)f_j(t)w_{ij}}{\overline{w}}, i = j. \end{cases}$$

743

744 <u>Inferring the ranges of possible fitness costs and dominance coefficients from empirical allele</u>

745 <u>frequency trajectories</u>

746 To estimate the fitness cost and dominance of malathion resistance in the malathion-free

747 environment, we analyzed the empirical frequency trajectories of these alleles in both the

748 untreated and treated populations after the removal of malathion. This approach allowed us to

749 constrain the range of possible parameters that could explain the observed frequencies of the

750 resistant alleles in both the treated and untreated populations. Assuming the resistant alleles share

751 the same selection (s) and dominance (h) coefficients, and further that the cost of resistance is

752 small (s<<1), the frequency dynamics follow

753 $$\partial_t f = s(f \cdot (1-f) \cdot (f + h(1-2f))),$$

754 allowing us to find s that would be consistent with the observed slope $\partial_t f$ of the frequency

755 trajectory for a given h[54].

756 To do that, we first bootstrapped the combined frequency trajectories of resistant alleles

757 in individual cages within each treatment group 10,000 times. For each set of bootstrapped

758 trajectories, we used linear regression (LinearRegression().fit function from the scikit-learn

759 Python library[55] to infer their slope. For a range of $h \in [0,1]$, we then calculated the bounds on s

760 by finding the values that correspond to the lower and upper bound of the 95% confidence

761 interval of the bootstrap distribution. To further constrain the range of possible parameters, we

762 similarly inferred the full distribution of s for each set of cages, and evaluated their overlap by

763 computing the joint likelihood function,

764 $$\mathcal{L} = \prod p(s),$$

765 where $p(s)$ is the probability density corresponding to a fixed value of s. Larger values of L

766 therefore correspond to more likely combinations of h and s given the observed frequency

767 dynamics.

768

769 **Characterize extent of forward and reverse sweep caused by *Ace* resistant alleles**

770 To assess how fluctuating organophosphate selection on the R2 and R3 *Ace* resistant alleles

771 affected genome-wide frequency trajectories of linked SNPs during and post-malathion

772 treatment, we employed a two-step approach. First, we used quasibinomial logistic regression to

773 estimate allele frequency shifts for genome-wide SNPs during malathion treatment (July 26 to

774 September 21, 2022) and post-treatment (September 21 to December 22, 2021). Second, we

775 developed a linked SNP selection procedure using linkage information from the inbred lines to

776 identify SNPs linked (Ace-linked) and not linked (control) to the sweeping R2 and R3 *Ace*

777 alleles across the genome. We used these sets of SNPs to quantify the extent of both the forward

778 *Ace* sweep during malathion treatment and the reverse *Ace* sweep post-treatment.

779

780 <u>Quasi-binomial logistic regression to estimate allele frequency differences in malathion-treated</u>

781 <u>and untreated populations during and after the malathion treatment</u>

782 To quantify allele frequency changes during malathion treatment (July 26 to September

783 21, 2022) and post-treatment (September 21 to December 22, 2021) in both treated and untreated

784 populations, we used a quasibinomial logistic regression approach[5,48]. This method models the

785 number of reads mapped to the alternative allele 'α' (relative to the reference allele 'A') at each

786 biallelic SNP for each pooled sample. To account for both the expected accuracy of HAFs as

787 well as pseudo-replication due to a fixed number of individuals in each sample [49], we estimated

788 an effective read depth reads (at each biallelic SNP for each pooled sample per population using

789 $$n_{eff} = \frac{\left((2 \times N \times EC) - 1\right)}{2 \times N + EC}$$

790 where N is the number of individuals per sample (100) and EC is the expected effective read

791 coverage based on the accuracy of HAF-pipe.

792 We then used a logit link implemented in a quasi-binomial logistic regression to model the

793 counts of the alternative allele 'α' $(C_a = HAF * neff)$ and reference allele 'A' $(C_A = (1 -$

794 $HAF) * neff)$ as a function of time in the malathion-treated and -untreated populations

795 $$logit(p_a) = log\left(\frac{p_a}{1 - p_a}\right) = b_0 + b_1 \times time + e$$

796 where p_a is probability of observing the allele 'α', while the coefficients b_0 and b_1 correspond to

797 the intercept and the effect of time, respectively. We fitted the model using the glm() function in

798 R (version 4.2.2) with family = 'quasibinomial'. To compute the allele frequency change (effect

799 size) between two time points (x_1 and x_2), we calculated

800 $$\Delta p = p_2 - p_1 = \frac{e^{(b_0 + b_1 \times x_2)}}{1 + e^{(b_0 + b_1 \times x_2)}} - \frac{e^{(b_0 + b_1 \times x_1)}}{1 + e^{(b_0 + b_1 \times x_1)}}$$

801

802 <u>Analysis of allele frequency changes of Ace-linked SNPs</u>

803 To quantify the extent of the forward and reverse *Ace* sweeps, we identified SNPs linked

804 to the sweeping R2 and R3 *Ace* alleles (*Ace*-linked), as well as unlinked (control) SNPs, using

805 whole genome data from the 76 sequenced Pennsylvania inbred lines (LNPA). First, we labeled

806 R2 and R3 *Ace* alleles as "R" and the remaining alleles (R1 and S) as "S", creating a binary

807 "R"/"S" *Ace* locus across the inbred lines. Among the inbred lines, 54 were homozygous "S", 5

808 heterozygous "R/S", and 17 homozygous "R". To select linked SNPs, we used the inbred lines

809 data to compute r^2 between the binary "R"/"S" *Ace* locus and every reported biallelic SNP in

810 the inbred LNPA lines as the squared correlation coefficient of allelic indicator variables[50]. We
811 initially retained SNPs with r2 > 0.03, a threshold frequency previously used to deem two loci
812 highly linked[6]. However, to avoid issues with low-frequency SNPs in finite populations, we
813 added an allele count condition. We selected SNPs with r2 > 0.03 that also have an allele present
814 in ≥60% of "R/R" lines and in ≤40% of “S/S” and “S/R” lines. This ensures selection of high-
815 frequency, well-assorted SNPs between "R" and "S" lines, which are more informative for sweep
816 analysis. This approach yielded 5672 Ace-linked SNPs across chromosomes 2, 3, and X. The
817 60% threshold was chosen as the highest value providing enough Ace-linked SNPs to uniformly
818 cover the genome, with consistent results when varied. Additionally, for each Ace-linked SNP,
819 we selected an unlinked control SNP with r2 < 0.01 with the binary "R"/"S" *Ace* locus. To ensure
820 comparable initial conditions, unlinked control SNPs were chosen within 500kb of their linked
821 counterpart and had an allele frequency within 0.05 of the Ace-linked SNP at the start of
822 malathion treatment in each cage. Finally, to ensure that we track the SNP alleles that are linked
823 specifically with the resistant lines, we transformed the alleles frequencies based on the sign of r
824 — the non-squared correlation coefficient of allelic indicator variables. If r between *Ace* and a
825 SNP is positive, then the alternative allele is assorted together with the resistant *Ace* alleles in the
826 inbred lines, if the sign of r is negative, then the reference allele is linked to resistant *Ace* alleles,
827 and in this case the alternative/reference labels were flipped, and the allele frequencies f_t were
828 transformed to 1-f_t. This process yielded 4793 matched unlinked control SNPs, fewer than the
829 linked SNPs due to the stringent matching criteria. To visualize the results, we aggregated SNPs
830 into 1Mb windows along the genome and used bootstrap resampling to compute median GLM-
831 estimated effect sizes and confidence intervals for Ace-linked and unlinked control SNPs
832 separately for both forward and reverse sweeps. We excluded the areas around the centromeres

833 and chromosome ends where less than 20 *Ace*-linked or control SNPs were observed. To
834 characterize the width of each sweep, we performed a two-sample Mann-Whitney U-test within
835 every 1Mb window across the chromosome and recorded the width of the contiguous range of
836 windows around *Ace* in which the median for *Ace*-linked SNPs is significantly greater than the
837 median for control SNPs at the 0.05 confidence level.

838 To quantify the reversal phenomenon during the *Ace* sweep post-malathion treatment, we
839 analyzed allele frequency changes for the same Ace-linked and unlinked control SNPs during the
840 post-treatment period (September 21 to December 22, 2021). We binned SNPs into
841 500Kb windows based on the genomic distance from the *Ace* locus on chromosome 3R and then
842 compared post-treatment to during-treatment frequency changes by plotting them against each
843 other within each bin. To quantify the reversal, we performed a joint linear regression for Ace-
844 linked and control SNPs and recorded which bins have shown a slope for Ace-linked SNPs
845 significantly more negative compared to control at the 0.05 confidence level.

846

847 **Data and Code availability**

848 The data and associated code for this study will become available after manuscript acceptance in
849 public repositories: Dryad (https://doi.org/10.5061/dryad.w0vt4b937) for the data and GitHub
850 (https://github.com/mkarageorgi/Beneficial_Dominance_Reversal) for the code. The sequences
851 of the LNPA inbred lines used to construct the baseline *D. melanogaster* population for the field
852 mesocosm experiment are available on NCBI under accession ID PRJNA722305. The raw
853 sequencing reads for pooled samples from the malathion-treated cages, collected during the field
854 mesocosm experiment, will be deposited in the SRA BioProject under accession number
855 PRJNA1031645. The raw sequencing reads for pooled samples from the untreated cages are
856 already available in the same SRA BioProject (PRJNA1031645).

Extended Data Figure 1

a

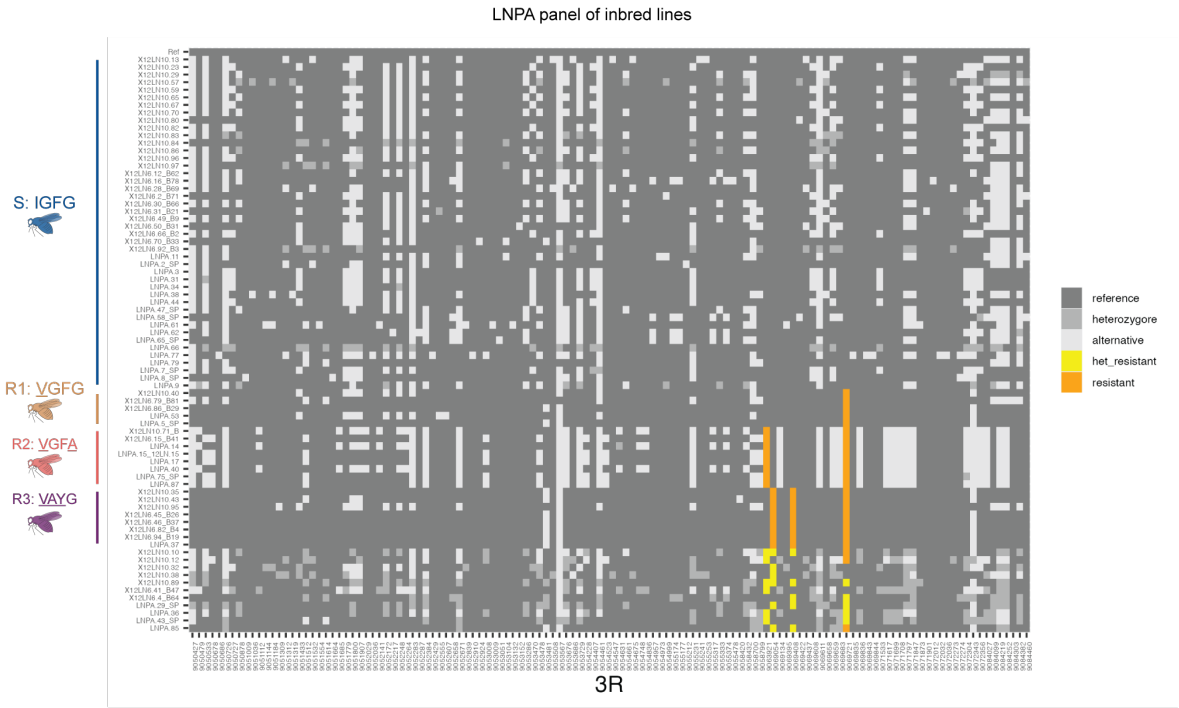

b

Ace haplotype	LNPA relative frequency (%)	DGRP relative frequency (%)
IGFG	63.16	54.15
VGFA	13.16	0.49
VAYG	12.50	30.73
VGFG	7.89	12.20
IGYG	1.32	0.98
IGFA	0.66	NA
VAFG	0.66	NA
VAYA	0.66	NA
IAFG	NA	1.46

Extended Data Figure 1. Sensitive and resistant *Ace* alleles in the panel of LNPA and DGRP inbred lines. a, Heatmap showing clustering of seventy-six *D. melanogaster* isogenic lines in the LNPA panel based on the sensitive or resistant *Ace* allele they carry (Ace-S: IGFG, Ace-R1: VGFG, Ace-R2: VGFA, Ace-R3: VAYG). The x-axis in the heatmap shows the genomic position on chromosome 3R around the *Ace* locus. Each row represents the *Ace* haplotype information of one isogenic line. Each column represents one biallelic exonic SNP at the *Ace* locus. Reference alleles are colored in dark grey, alternative alleles are colored in light grey, heterozygotes in medium grey. For the resistance mutations, alleles coding for the resistance mutations are colored in orange, alternative in grey, and heterozygotes in yellow. **b,** Table showing frequency of the sensitive and each of the resistant *Ace* alleles carrying different resistance haplotypes in the panels of LNPA and DGRP inbred lines.

Extended Data Figure 2

a

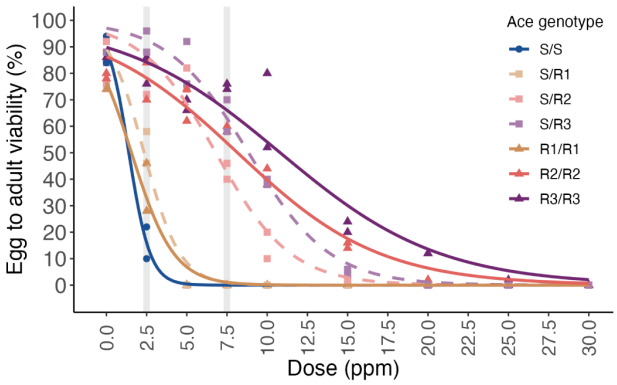

b

Dose response curve analysis for each Ace genotype

Genotype	LD50	std.error	statistic	p.value
SS	1.39	0.18	7.79	3.7768e-12
R1R1	1.56	0.20	7.68	6.3407e-12
R2R2	8.16	0.40	20.41	7.7563e-40
R3R3	10.81	0.45	23.96	3.3625e-46
SR1	2.34	0.19	12.49	3.0000e-23
SR2	6.80	0.26	25.89	2.1374e-49
SR3	8.84	0.30	29.95	1.3764e-55

Extended Data Figure 2. Comparison of malathion resistance among the *Ace* genotypes. a, Lab measurements of egg to adult viability in recombinant populations carrying different *Ace* genotypes on standard Drosophila media with a range of malathion concentrations (n= 2 technical replicates per genotype for each malathion doses, 50 eggs per replicate). Four-parameter logistic models fitted to data of each *Ace* genotype. The shaded areas highlight viability of each genotype at malathion doses (2.5ppm and 7.5 ppm) applied in the field mesocosm experiment. **b,** Table with estimated LD_{50} values for each *Ace* genotype from four-parameter logistic dose-response model (see also **Methods**).

Extended Data Figure 3

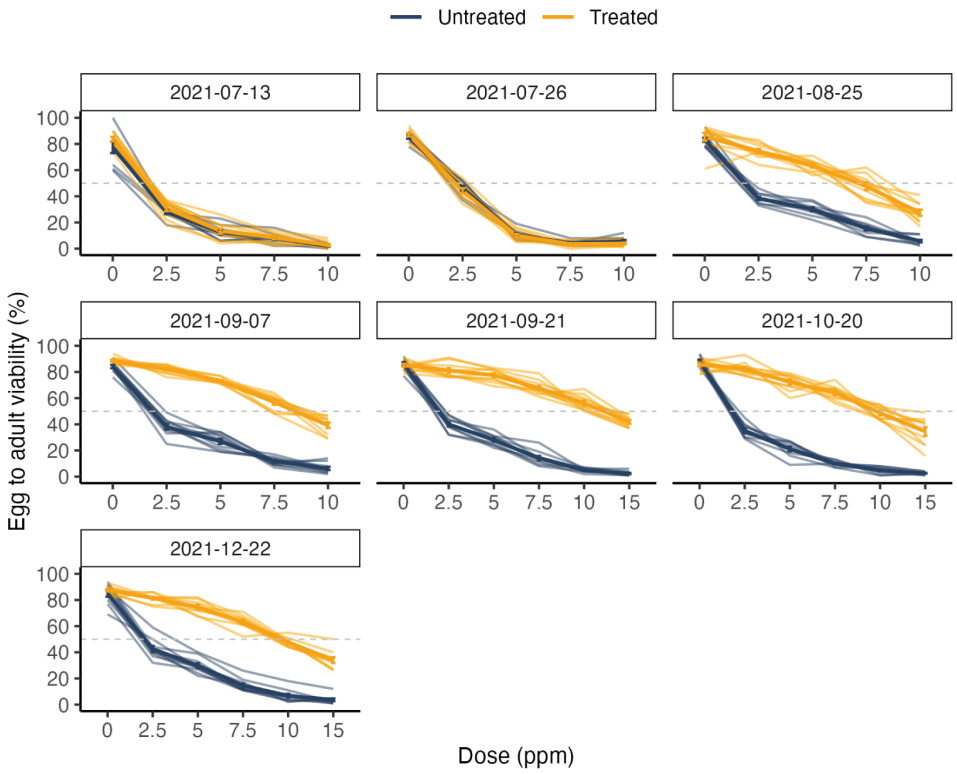

Extended Data Figure 3. Tracking evolution of malathion resistance in the field mesocosm experiment. Egg-adult survival on diets with a range of malathion concentrations as measured after two generations of common garden rearing throughout the field mesocosm experiment. Light lines and points show the mean egg-adult survival for individual malathion-treated (orange) and untreated (blue) populations (n = 2 technical replicates, 50 eggs per replicate). Dark lines and points represent the mean ± s.e.m. from all populations for each treatment group (n = 10 populations per treatment group). Further information on experimental design can be found in **Methods**.

Extended Data Figure 4

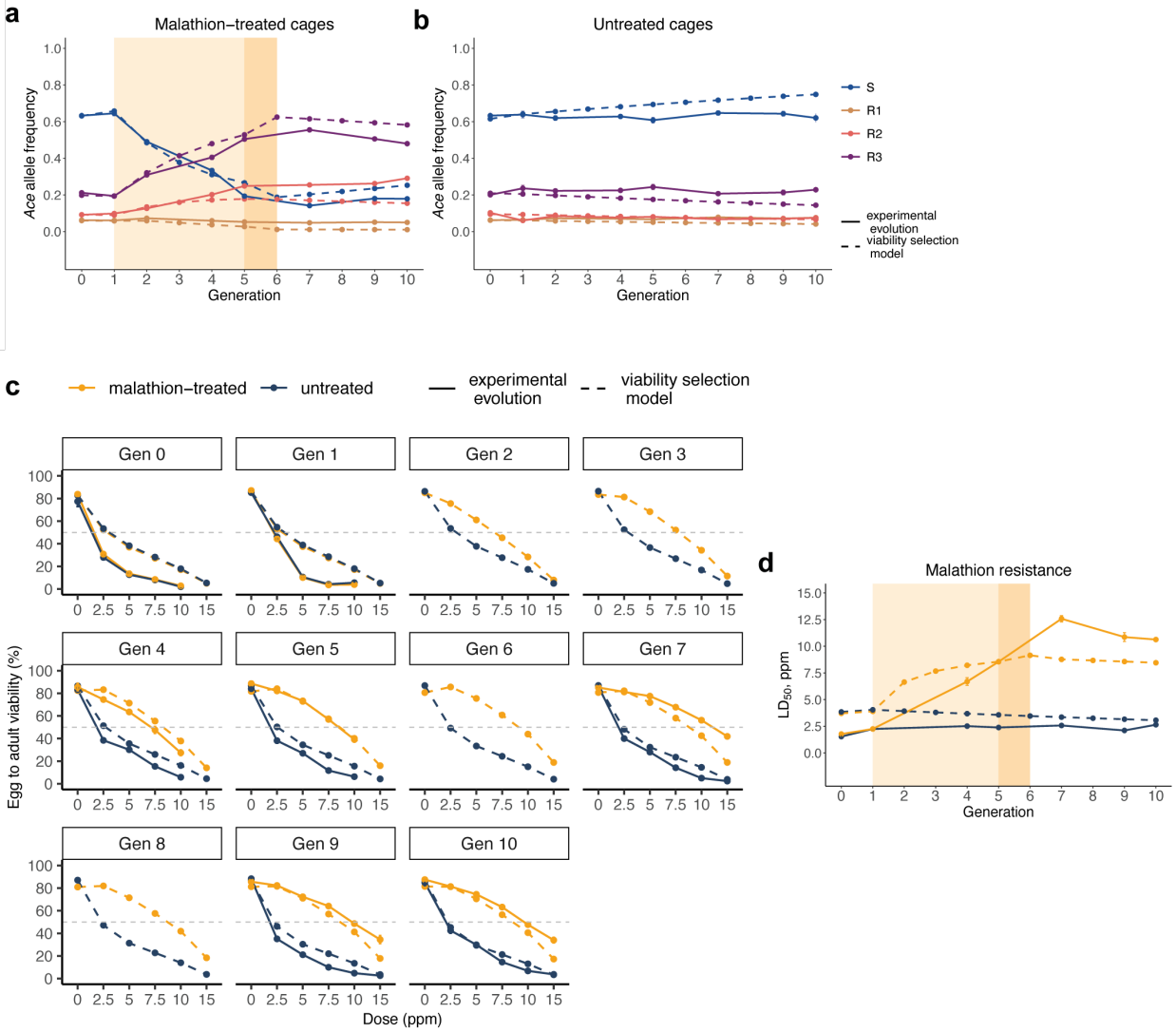

863

Extended Data Figure 4. Modeling the impact of viability selection on *Ace* allele frequency dynamics and malathion resistance in the field mesocosm experiment. **a-b,** Comparison between the observed *Ace* allele frequency trajectories over 10 generations in the malathion-treated (**a**) and untreated (**b**) populations from the field mesocosm experiment (mean ± s.e.m.) and the expected trajectories from simulations based on a viability selection model using laboratory-derived parameters. See **Methods** for details about the viability selection model. **c-d,** Comparison between the observed egg-to-adult survival across a range of malathion concentrations (**c**) and the evolution of malathion resistance (LD_{50}, ppm) (**d**) over 10 generations in the field mesocosm experiment (mean ± s.e.m.), and the expected results from the same model simulations. Dashed lines represent the expected values from the viability selection model, while solid lines represent the observed data from the field experiment. Generations were estimated based on a degree-day model starting from the first sampling point (July 13, 2021). In all plots, points correspond to each generation and estimated time point, and are connected by lines for visualization.

Extendend Data Table 1

Effect estimates from linear model analysis for LD50

Parameter	LD50	Std.Error	P.value
SS mean	1.39	0.19	-
SR1 mean	2.34	0.13	-
R1R1 mean	1.56	0.14	-
SS vs. SR1	-0.93	0.34	0.0063
SS vs. R1R1	-0.17	0.37	0.646
SR1 vs. R1R1	0.76	0.39	0.0516
SR1 - (SS + R1R1)/2 (additivity)	0.76	0.32	1e-16
(R1R1 - SS) / R1R1 (selection, s)	-0.25	0.29	0.751
(SR1 - SS) / (R1R1 - SS) (dominance, h)	-1.29	5.10	0.751
SR2 mean	6.80	0.24	-
R2R2 mean	8.16	0.36	-
SS vs. SR2	-5.38	0.36	0
SS vs. R2R2	-6.72	0.42	0
SR2 vs. R2R2	-1.34	0.45	0.003
SR2 - (SS + R2R2)/2 (additivity)	1.87	0.35	1e-16
(R2R2 - SS) / R2R2 (selection, s)	3.83	1.05	1e-16
(SR2 - SS) / (R2R2 - SS) (dominance, h)	0.78	0.06	1e-16
SR3 mean	8.84	0.32	-
R3R3 mean	10.81	0.49	-
SS vs. SR3	-7.41	0.36	0
SS vs. R3R3	-9.37	0.79	0
SR3 vs. R3R3	-1.96	0.80	0.0145
SR3 - (SS + R3R3)/2 (additivity)	2.59	0.48	1e-16
(R3R3 - SS) / R3R3 (selection, s)	5.64	1.45	1e-16
(SR3 - SS) / (R3R3 - SS) (dominance, h)	0.77	0.07	1e-16

Extendend Data Table 2

Effect estimates from logistic model analysis for viability

Parameter	Viability	Std.Error	Lower.CI	Upper.CI	P.value
SS mean	0.89	0.01	-	-	-
SR1 mean	0.86	0.02	-	-	-
R1R1 mean	0.76	0.02	-	-	-
SS vs. SR1	1.42	0.27	-	-	0.0702
SS vs. R1R1	2.61	0.47	-	-	<.0001
SR1 vs. R1R1	1.84	0.30	-	-	4e-04
SR1 - (SS + R1R1)/2 (additivity)	0.03	0.02	-0.02	0.07	0.214
(R1R1 - SS) / R1R1 (selection, s)	-0.15	0.03	-0.2	-0.09	0.001
(SR1 - SS) / (R1R1 - SS) (dominance, h)	0.29	0.20	-0.15	0.64	0.214
SR2 mean	0.87	0.02	-	-	-
R2R2 mean	0.74	0.02	-	-	-
SS vs. SR2	1.28	0.25	-	-	0.205
SS vs. R2R2	2.96	0.53	-	-	<.0001
SR2 vs. R2R2	2.31	0.39	-	-	<.0001
SR2 - (SS + R2R2)/2 (additivity)	0.05	0.02	0.01	0.1	0.027
(R2R2 - SS) / R2R2 (selection, s)	-0.17	0.05	-0.28	-0.09	0.001
(SR2 - SS) / (R2R2 - SS) (dominance, h)	0.17	0.15	-0.15	0.45	0.027
SR3 mean	0.86	0.02	-	-	-
R3R3 mean	0.78	0.02	-	-	-
SS vs. SR3	1.42	0.27	-	-	0.0702
SS vs. R3R3	2.43	0.44	-	-	<.0001
SR3 vs. R3R3	1.72	0.29	-	-	0.0018
SR3 - (SS + R3R3)/2 (additivity)	0.02	0.02	-0.02	0.06	0.286
(R3R3 - SS) / R3R3 (selection, s)	-0.13	0.02	-0.18	-0.08	0.001
(SR3 - SS) / (R3R3 - SS) (dominance, h)	0.32	0.19	-0.15	0.67	0.286

865

Extendend Data Table 3

Effect estimates from linear model analysis for fecundity

Parameter	Fecundity	Std.Error	Lower.CI	Upper.CI	P.value
SS mean	200.22	11.99	-	-	-
SR1 mean	165.33	14.01	-	-	-
R1R1 mean	136.50	14.86	-	-	-
SS vs. SR1	34.89	19.81	-	-	0.14
SS vs. R1R1	63.72	20.42	-	-	0.01
SR1 vs. R1R1	28.83	20.42	-	-	0.17
SR1 - (SS + R1R1)/2 (additivity)	-3.03	17.26	-36.62	31.59	0.879
(R1R1 - SS) / R1R1 (selection, s)	-0.32	0.09	-0.48	-0.12	0.003
(SR1 - SS) / (R1R1 - SS) (dominance, h)	0.55	0.40	-0.07	1.32	0.881
SR2 mean	187.60	13.64	-	-	-
R2R2 mean	167.78	14.37	-	-	-
SS vs. SR2	12.62	19.81	-	-	0.53
SS vs. R2R2	32.44	20.33	-	-	0.37
SR2 vs. R2R2	19.82	19.81	-	-	0.49
SR2 - (SS + R2R2)/2 (additivity)	3.60	18.42	-33.15	43.16	0.834
(R2R2 - SS) / R2R2 (selection, s)	-0.16	0.09	-0.33	0.03	0.093
(SR2 - SS) / (R2R2 - SS) (dominance, h)	0.39	4.09	-2.3	3.23	0.842
SR3 mean	202.00	12.71	-	-	-
R3R3 mean	106.44	11.99	-	-	-
SS vs. SR3	-1.78	17.47	-	-	0.92
SS vs. R3R3	93.78	16.95	-	-	<.0001
SR3 vs. R3R3	95.56	17.47	-	-	<.0001
SR3 - (SS + R3R3)/2 (additivity)	48.67	12.84	22.41	73.56	1e-16
(R3R3 - SS) / R3R3 (selection, s)	-0.47	0.07	-0.59	-0.31	0.001
(SR3 - SS) / (R3R3 - SS) (dominance, h)	-0.02	0.19	-0.48	0.29	0.001

866

Extendend Data Table 4

Extended Data Table 4.1 Effect of time on malathion resistance (LD50) in treated cages

	During treatment				*After treatment*			
Predictors	**Estimates**	**std. Error**	**Statistic**	**p**	**Estimates**	**std. Error**	**Statistic**	**p**
Intercept	-3.02 ***	0.46	-6.58	**<0.001**	15.56 ***	1.09	14.29	**<0.001**
Time	2.48 ***	0.10	24.26	**<0.001**	-0.57 ***	0.14	-3.96	**0.001**
Random Effects								
σ^2	0.91				0.98			
τ_{00}	$0.00_{Treatment_Cage}$				$0.24_{Treatment_Cage}$			
ICC					0.20			
N	$10_{Treatment_Cage}$				$10_{Treatment_Cage}$			
Observations	40				30			
Marginal R^2 / Conditional R^2	0.938 / NA				0.302 / 0.441			
AIC	122.513				101.066			

** p<0.05 ** p<0.01 *** p<0.001*

Extended Data Table 4.2 Effect of time on malathion resistance (LD50) in untreated cages

	Beginning of treatment to end of experiment			
Predictors	**Estimates**	**std. Error**	**Statistic**	**p**
Intercept	2.27 ***	0.15	14.91	**<0.001**
Time	0.03	0.02	1.07	0.288
Random Effects				
σ^2	0.16			
$\tau_{00\ Treatment_Cage}$	0.03			
ICC	0.15			
$N_{Treatment_Cage}$	10			
Observations	59			
Marginal R^2 / Conditional R^2	0.017 / 0.166			
AIC	83.651			

** p<0.05 ** p<0.01 *** p<0.001*

867

Extendend Data Table 5

Extended Data Table 5.1 Effect of time on S (IGFG) frequency in treated cages

	During treatment				*After treatment*			
Predictors	**Estimates**	**std. Error**	**Statistic**	**p**	**Estimates**	**std. Error**	**Statistic**	**p**
Intercept	0.88 ***	0.02	49.15	**<0.001**	0.04	0.05	0.74	0.468
Time	-0.13 ***	0.00	-30.81	**<0.001**	0.02 *	0.01	2.64	**0.014**
Random Effects								
σ^2	0.00				0.00			
τ_{00}	0.00_{cage}				0.00_{cage}			
N	10_{cage}				10_{cage}			
Observations	50				30			
Marginal R^2 / Conditional R^2	0.951 / NA				0.194 / NA			
AIC	-148.876				-97.774			

** p<0.05 ** p<0.01 *** p<0.001*

Extended Data Table 5.2 Effect of time on R1 (VGFG) frequency in treated cages

	During treatment				*After treatment*			
Predictors	**Estimates**	**std. Error**	**Statistic**	**p**	**Estimates**	**std. Error**	**Statistic**	**p**
Intercept	0.08 ***	0.00	16.13	**<0.001**	0.04 **	0.01	3.09	**0.005**
Time	-0.00 ***	0.00	-4.05	**<0.001**	0.00	0.00	0.46	0.651
Random Effects								
σ^2	0.00				0.00			
τ_{00}	0.00_{cage}				0.00_{cage}			
ICC					0.25			
N	10_{cage}				10_{cage}			
Observations	50				30			
Marginal R^2 / Conditional R^2	0.251 / NA				0.005 / 0.250			
AIC	-276.043				-162.492			

** p<0.05 ** p<0.01 *** p<0.001*

Extended Data Table 5.3 Effect of time on R2 (VGFA) frequency in treated cages

	During treatment				*After treatment*			
Predictors	**Estimates**	**std. Error**	**Statistic**	**p**	**Estimates**	**std. Error**	**Statistic**	**p**
Intercept	0.01	0.01	0.93	0.356	0.14 **	0.04	3.39	**0.002**
Time	0.04 ***	0.00	13.93	**<0.001**	0.02 **	0.01	3.03	**0.006**
Random Effects								
σ^2	0.00				0.00			
τ_{00}	0.00_{cage}				0.00_{cage}			
N	10_{cage}				10_{cage}			
Observations	50				30			
Marginal R^2 / Conditional R^2	0.798 / NA				0.240 / NA			
AIC	-178.169				-107.043			

** p<0.05 ** p<0.01 *** p<0.001*

Extended Data Table 5.4 Effect of time on R3 (VAYG) frequency in treated cages

	During treatment				*After treatment*			
Predictors	**Estimates**	**std. Error**	**Statistic**	**p**	**Estimates**	**std. Error**	**Statistic**	**p**
Intercept	0.03	0.01	1.88	0.067	0.78 ***	0.05	15.18	**<0.001**
Time	0.09 ***	0.00	27.59	**<0.001**	-0.04 ***	0.01	-5.18	**<0.001**
Random Effects								
σ^2	0.00				0.00			
τ_{00}	0.00_{cage}				0.00_{cage}			
ICC	0.04							
N	10_{cage}				10_{cage}			
Observations	50				30			
Marginal R^2 / Conditional R^2	0.937 / 0.940				0.481 / NA			
AIC	-170.172				-96.128			

** p<0.05 ** p<0.01 *** p<0.001*

868

Extendend Data Table 6

Extended Data Table 6.1 Effect of time on S (IGFG) haplotype frequency in untreated cages

	Beginning of treatment to end of experiment			
Predictors	**Estimates**	**std. Error**	**Statistic**	**p**
Intercept	0.63 ***	0.02	39.49	**<0.001**
Time	0.00	0.00	0.21	0.838
Random Effects				
σ^2		0.00		
$\tau_{00\ cage}$		0.00		
ICC		0.03		
N_{cage}		10		
Observations		69		
Marginal R^2 / Conditional R^2		0.001 / 0.032		
AIC		-196.762		

** p<0.05 ** p<0.01 *** p<0.001*

Extended Data Table 6.2 Effect of time on R1 (VGFG) haplotype frequency in untreated cages

	Beginning of treatment to end of experiment			
Predictors	**Estimates**	**std. Error**	**Statistic**	**p**
Intercept	0.06 ***	0.00	14.68	**<0.001**
Time	0.00	0.00	1.91	0.061
Random Effects				
σ^2		0.00		
$\tau_{00\ cage}$		0.00		
N_{cage}		10		
Observations		69		
Marginal R^2 / Conditional R^2		0.051 / NA		
AIC		-370.061		

** p<0.05 ** p<0.01 *** p<0.001*

Extended Data Table 6.3 Effect of time on R2 (VGFA) haplotype frequency in untreated cages

	Beginning of treatment to end of experiment			
Predictors	**Estimates**	**std. Error**	**Statistic**	**p**
Intercept	0.07 ***	0.01	9.08	**<0.001**
Time	-0.00	0.00	-0.02	0.985
Random Effects				
σ^2		0.00		
$\tau_{00\ cage}$		0.00		
ICC		0.02		
N_{cage}		10		
Observations		69		
Marginal R^2 / Conditional R^2		0.000 / 0.024		
AIC		-285.686		

** p<0.05 ** p<0.01 *** p<0.001*

Extended Data Table 6.4 Effect of time on R3 (VAYG) haplotype frequency in untreated cages

	Beginning of treatment to end of experiment			
Predictors	**Estimates**	**std. Error**	**Statistic**	**p**
Intercept	0.24 ***	0.01	17.99	**<0.001**
Time	-0.00	0.00	-0.86	0.392
Random Effects				
σ^2		0.00		
$\tau_{00\ cage}$		0.00		
ICC		0.05		
N_{cage}		10		
Observations		69		
Marginal R^2 / Conditional R^2		0.010 / 0.064		
AIC		-222.940		

** p<0.05 ** p<0.01 *** p<0.001*

869

870 **References**

871 1. Hedrick, P. W. Genetic polymorphism in heterogeneous environments: The age of
872 genomics. *Annu. Rev. Ecol. Evol. Syst.* **37**, 67–93 (2006).
873 2. Johnson, O. L., Tobler, R., Schmidt, J. M. & Huber, C. D. Fluctuating selection and the
874 determinants of genetic variation. *Trends Genet.* **39**, 491–504 (2023).
875 3. Bergland, A. O., Behrman, E. L., O'Brien, K. R., Schmidt, P. S. & Petrov, D. A. Genomic
876 evidence of rapid and stable adaptive oscillations over seasonal time scales in Drosophila.
877 *PLoS Genet.* **10**, e1004775 (2014).
878 4. Machado, H. E. *et al.* Broad geographic sampling reveals the shared basis and
879 environmental correlates of seasonal adaptation in Drosophila. *Elife* **10**, (2021).
880 5. Rudman, S. M. *et al.* Direct observation of adaptive tracking on ecological time scales in
881 Drosophila. *Science* **375**, eabj7484 (2022).
882 6. Bitter, M. C. *et al.* Continuously fluctuating selection reveals fine granularity of adaptation.
883 *Nature* **634**, 389–396 (2024).
884 7. Haldane, J. B. S. & Jayakar, S. D. Polymorphism due to selection of varying direction. *J.*
885 *Genet.* **58**, 237–242 (1963).
886 8. Hedrick, P. W. Genetic variation in a heterogeneous environment. II. Temporal
887 heterogeneity and directional selection. *Genetics* **84**, 145–157 (1976).
888 9. Wittmann, M. J., Bergland, A. O., Feldman, M. W., Schmidt, P. S. & Petrov, D. A.
889 Seasonally fluctuating selection can maintain polymorphism at many loci via segregation
890 lift. *Proc Natl Acad Sci U S A* **114**, E9932–E9941 (2017).
891 10. Connallon, T. & Chenoweth, S. F. Dominance reversals and the maintenance of genetic
892 variation for fitness. *PLOS Biology* **17**, e3000118 (2019).

11. Grieshop, K., Ho, E. K. H. & Kasimatis, K. R. Dominance reversals: the resolution of genetic conflict and maintenance of genetic variation. *Proceedings of the Royal Society B* (2024) doi:10.1098/rspb.2023.2816.

12. Wright, S. Physiological and evolutionary theories of dominance. *Am. Nat.* **68**, 24–53 (1934).

13. Fournier, D. & Mutero, A. Modification of acetylcholinesterase as a mechanism of resistance to insecticides. *C, No. I, pp.* **19**, 31 (1994).

14. Hall, J. C. & Kankel, D. R. Genetics of acetylcholinesterase in Drosophila melanogaster. *Genetics* **83**, 517–535 (1976).

15. Aldridge, W. N. Some properties of specific cholinesterase with particular reference to the mechanism of inhibition by diethyl p-nitrophenyl thiophosphate (E 605) and analogues. *Biochem. J.* **46**, 451–460 (1950).

16. Lenormand, T., Bourguet, D., Guillemaud, T. & Raymond, M. Tracking the evolution of insecticide resistance in the mosquito Culex pipiens. *Nature* **400**, 861–864 (1999).

17. Miyo, T., Akai, S. & Ogumma, Y. Seasonal fluctuation in susceptibility to insecticides within natural populations of Drosophila melanogaster: empirical observations of fitness costs of insecticide resistance.

18. Miyo, T., Oguma, Y. & Charlesworth, B. Seasonal fluctuation in susceptibility to insecticides within natural populations of Drosophila melanogaster. II. Features of genetic variation in susceptibility to organophosphate insecticides within natural populations of D. melanogaster. *Genes Genet. Syst.* **81**, 273–285 (2006).

19. Bourguet, D. & Raymond, M. The molecular basis of dominance relationships: the case of some recent adaptive genes. *J. Evol. Biol.* **11**, 103–122 (1998).

916 20. Muralidhar, P. & Veller, C. Dominance shifts increase the likelihood of soft selective
917 sweeps. *Evolution* **76**, 966–984 (2022).
918 21. Labbé, P. *et al.* GENE-dosage effects on fitness in recent adaptive duplications: ace-1 in the
919 mosquito Culex pipiens. *Evolution* **68**, 2092–2101 (2014).
920 22. Menozzi, P., Shi, M. A., Lougarre, A., Tang, Z. H. & Fournier, D. Mutations of
921 acetylcholinesterase which confer insecticide resistance in Drosophila melanogaster
922 populations. *BMC Evol. Biol.* **4**, 4 (2004).
923 23. Karasov, T., Messer, P. W. & Petrov, D. A. Evidence that adaptation in Drosophila is not
924 limited by mutation at single sites. *PLoS Genet.* **6**, e1000924 (2010).
925 24. Shi, M. A. *et al.* Acetylcholinesterase alterations reveal the fitness cost of mutations
926 conferring insecticide resistance. *BMC Evol. Biol.* **4**, 5 (2004).
927 25. Mackay, T. F. C. *et al.* The Drosophila melanogaster Genetic Reference Panel. *Nature* **482**,
928 173–178 (2012).
929 26. Kapun, M. *et al.* Drosophila Evolution over Space and Time (DEST): A new population
930 genomics resource. *Mol. Biol. Evol.* **38**, 5782–5805 (2021).
931 27. FAO. Pesticides use and trade, 1990–2022. (2024).
932 28. Paaby, A. B., Bergland, A. O., Behrman, E. L. & Schmidt, P. S. A highly pleiotropic amino
933 acid polymorphism in the Drosophila insulin receptor contributes to life-history adaptation.
934 *Evolution* **68**, 3395–3409 (2014).
935 29. Wittmann, M. J., Mousset, S. & Hermisson, J. Modeling the genetic footprint of fluctuating
936 balancing selection: from the local to the genomic scale. *Genetics* **223**, iyad022 (2023).
937 30. Kaplan, N., Hudson, R. & Langley, C. The 'hitchhiking effect' revisited. *Genetics* **123**,
938 887–899 (1989).

939 31. Langmüller, A. M. *et al.* Fitness effects for Ace insecticide resistance mutations are
940 determined by ambient temperature. *BMC Biol.* **18**, 157 (2020).
941 32. Johnston, S. E. *et al.* Life history trade-offs at a single locus maintain sexually selected
942 genetic variation. *Nature* **502**, 93–95 (2013).
943 33. Barson, N. J. *et al.* Sex-dependent dominance at a single locus maintains variation in age at
944 maturity in salmon. *Nature* **528**, 405–408 (2015).
945 34. Pfenninger, M. & Foucault, Q. Population genomic time series data of a natural population
946 suggests adaptive tracking of fluctuating environmental changes. *Integr. Comp. Biol.* **62**,
947 1812–1826 (2022).
948 35. Pfenninger, M., Foucault, Q., Waldvogel, A.-M. & Feldmeyer, B. Selective effects of a
949 short transient environmental fluctuation on a natural population. *Mol. Ecol.* **32**, 335–349
950 (2023).
951 36. Mutero, A., Pralavorio, M., Bride, J. M. & Fournier, D. Resistance-associated point
952 mutations in insecticide-insensitive acetylcholinesterase. *Proc. Natl. Acad. Sci. U. S. A.* **91**,
953 5922–5926 (1994).
954 37. Harel, M. *et al.* Three-dimensional structures of Drosophila melanogaster
955 acetylcholinesterase and of its complexes with two potent inhibitors. *Protein Sci.* **9**, 1063–
956 1072 (2000).
957 38. Ritz, C., Baty, F., Streibig, J. C. & Gerhard, D. Dose-Response Analysis Using R. *PLoS*
958 *One* **10**, e0146021 (2015).
959 39. Tilk, S. *et al.* Accurate Allele Frequencies from Ultra-low Coverage Pool-Seq Samples in
960 Evolve-and-Resequence Experiments. *G3* **9**, 4159–4168 (2019).
961 40. Miyo, T. & Oguma, Y. Negative correlations between resistance to three organophosphate

962 insecticides and productivity within a natural population of Drosophila melanogaster
963 (Diptera: Drosophilidae). *J. Econ. Entomol.* **95**, 1229–1238 (2002).
964 41. Singh, R. S. & Morton, R. A. Selection for malathion-resistance in Drosophila
965 melanogaster. *Can. J. Genet. Cytol.* **23**, 355–369 (1981).
966 42. Li, H. & Durbin, R. Fast and accurate short read alignment with Burrows-Wheeler
967 transform. *Bioinformatics* **25**, 1754–1760 (2009).
968 43. Kessner, D., Turner, T. L. & Novembre, J. Maximum likelihood estimation of frequencies
969 of known haplotypes from pooled sequence data. *Mol. Biol. Evol.* **30**, 1145–1158 (2013).
970 44. Gillespie, J. H. *Population Genetics*. (Johns Hopkins University Press, Baltimore, MD,
971 2004).
972 45. Behrman, E. L. & Schmidt, P. How predictable is rapid evolution? (2022)
973 doi:10.1101/2022.10.27.514123.
974 46. Ewens, W. J. *Mathematical Population Genetics 1: Theoretical Introduction*. (Springer,
975 New York, NY, 2010).
976 47. Pedregosa, F. *et al.* Scikit-learn: Machine Learning in Python. *arXiv [cs.LG]* (2012).
977 48. Wiberg, R. A. W., Gaggiotti, O. E., Morrissey, M. B. & Ritchie, M. G. Identifying
978 consistent allele frequency differences in studies of stratified populations. *Methods Ecol.*
979 *Evol.* **8**, 1899–1909 (2017).
980 49. Feder, A. F., Petrov, D. A. & Bergland, A. O. LDx: estimation of linkage disequilibrium
981 from high-throughput pooled resequencing data. *PLoS One* **7**, e48588 (2012).
982 50. VanLiere, J. M. & Rosenberg, N. A. Mathematical properties of the r2 measure of linkage
983 disequilibrium. *Theor. Popul. Biol.* **74**, 130–137 (2008).